Evaluation and uncertainty investigation of the NO_2, CO and NH_3 modeling over China under the framework of MICS-Asia III

Lei Kong[1,3], Xiao Tang[2,3], Jiang Zhu[1,3], Zifa Wang[2,3], Joshua S. Fu[4], Xuemei Wang[5], Syuichi Itahashi[6,7], Kazuyo Yamaji[8], Tatsuya Nagashima[9], Hyo-Jung Lee[10], Cheol-Hee Kim[10], Chuan-Yao Lin[11], Lei Chen[2,3], Meigen Zhang[2,3], Zhining Tao[12,13], Jie Li[2,3], Mizuo Kajino[14,15], Hong Liao[16], Zhe Wang[17,2], Kengo Sudo[18] Yuesi Wang[2,3], Yuepeng Pan[2,3], Guiqian Tang[2,3], Meng Li[19,20], Qizhong Wu[21,22]; Baozhu Ge[2,3], Gregory R. Carmichael[23]

[1]ICCES, Institute of Atmospheric Physics, Chinese Academy of Sciences, Beijing, 100029, China
[2]LAPC, Institute of Atmospheric Physics, Chinese Academy of Sciences, Beijing, 100029, China
[3]University of Chinese Academy of Sciences, Beijing, 100049, China
[4]Department of Civil and Environmental Engineering, University of Tennessee, Knoxville, TN, 37996, USA
[5]Institite for Environment and Climate Research, Jinan University, Guangzhou, 510632, China
[6]Central Research Institute of Electric Power Industry, Abiko, Chiba, 270-1194, Japan
[7]Department of Marine, Earth, and Atmospheric Sciences, North Carolina State University, Raleigh, NC 27607, USA
[8]Graduate School of Maritime Sciences, Kobe University, Kobe, Hyogo 658-0022, Japan
[9]National Institute for Environmental Studies, Onogawa, Tsukuba 305-8506, Japan
[10]Department of Atmospheric Sciences, Pusan National University, Busan, 46241, South Korea
[11]Research Center for Environmental Changes, Academia Sinica, Taipei, 115, Taiwan
[12]Universities Space Research Association, Columbia, MD, USA
[13]NASA Goddard Space Flight Center, Greenbelt, MD, 130, USA
[14]Meteorological Research Institute, Japan Meteorological Agency, Tsukuba, Ibaraki, 305-0052, Japan
[15]Faculty of Life and Environmental Sciences, University of Tsukuba, Tsukuba, Ibaraki, 305-8577, Japan
[16]School of Environmental Science and Engineering, Nanjing University of Information Science & Technology, Nanjing 210044, China
[17]Research Institute for Applied Mechanics (RIAM), Kyushu University, Fukuoka, Japan
[18]Graduate School of Environmental Studies, Nagoya University, Nagoya, Japan
[19]Ministry of Education Key laboratory for Earth System Modeling, Department of Earth System Science, Tsinghua University, Beijing, 100084, China
[20]Multiphase Chemistry Department, Max Planck Institute for Chemistry, Mainz, 55128, Germany
[21]College of Global Change and Earth System Science, Beijing Normal University, Beijing 100875, China
[22]Joint Centre for Global Changes Studies, Beijing Normal University, Beijing 100875, China
[23]Center for Global and Regional Environmental Research, University of Iowa, Iowa City, IA, 52242, USA

Correspondence to: Xiao Tang(tangxiao@mail.iap.ac.cn)

Abstract. Despite the significant progress in improving the chemical transport models (CTMs), applications of these modeling endeavours are still subject to the large and complex model uncertainty. Model Inter-Comparison Study for Asia III (MICS-Asia III) has provided the opportunity to assess the capability and uncertainty of current CTMs in East Asia applications. In this study, we have evaluated the multi-model simulations of nitrogen dioxide (NO_2), carbon monoxide (CO) and ammonia (NH_3) over China under the framework of MICS-Asia III. Thirteen modeling results, provided by several independent groups from different countries/regions, were used in this study. Most of these models used some modeling domain with a horizontal resolution of 45km, and were driven by common emission inventories and meteorological inputs. New observations over North

China Plain (NCP) and Pearl River Delta (PRD) regions were also available in MICS-Asia III, allowing the model evaluations over highly industrialized regions. The evaluation results show that most models well captured the monthly and spatial patterns of NO_2 concentrations in the NCP region though NO_2 levels were slightly underestimated. Relatively poor performance in NO_2 simulations was found in the PRD region with larger root mean square error and lower spatial correlation coefficients, which may be related to the coarse resolution or inappropriate spatial allocations of the emission inventories in the PRD region. All models significantly underpredicted CO concentrations in both the NCP and PRD regions, with annual mean concentrations 65.4% and 61.4% underestimated by the ensemble mean. Such large underestimations suggest that CO emissions might be underestimated in current emission inventory. In contrast to the good skills in simulating the monthly variations of NO_2 and CO concentrations, all models failed to reproduce the observed monthly variations of NH_3 concentrations in the NCP region. Most models mismatched the observed peak in July and showed negative correlation coefficients with observations, which may be closely related to the uncertainty in the monthly variations of NH_3 emissions and the NH_3 gas-aerosol partitioning. Finally, model inter-comparisons have been conducted to quantify the impacts of model uncertainty on the simulations of these gases which are shown increase with the reactivity of species. Models contained more uncertainty in the NH_3 simulations. This suggests that for some highly active and/or short-lived primary pollutants, like NH_3, model uncertainty can also take a great part in the forecast uncertainty besides the emission uncertainty. Based on these results, some recommendations are made for future studies.

1 Introduction

As the rapid growth in East Asia's economy with surging energy consumption and emissions, air pollution has become an increasingly important scientific topic and political concern in East Asia due to its significant environmental and health effects (Anenberg et al., 2010;Lelieveld et al., 2015). Chemical transport models (CTMs), serving as a critical tool in both the scientific research and policy makings, have been applied into various air quality issues, such as air quality prediction, long-range transport of atmospheric pollutants, development of emission control strategies and understanding of observed chemical phenomena (e.g. Cheng et al., 2016;Li et al., 2017a;Lu et al., 2017;Ma et al., 2019;Tang et al., 2011;Xu et al., 2019;Zhang et al., 2019). Nevertheless, air quality modeling remains a challenge due to the multi-scale and non-linear nature of the complex atmospheric processes (Carmichael et al., 2008). It still suffers from large uncertainties related to the missing or poorly parameterized physical and chemical processes, inaccurate and/or incomplete emission inventories as well as the poorly represented initial and boundary conditions (Carmichael et al., 2008;Dabberdt and Miller, 2000;Fine et al., 2003;Gao et al., 1996;Mallet and Sportisse, 2006). Understanding such uncertainties and their impacts on the air quality modeling is of great importance in assessing the robustness of models for their applications in scientific research and operational use.

There are specific techniques to assess these uncertainties. Monte Carlo simulations, based on different values of model parameters or input fields sampled from a predefined probability density function (PDF), can provide an approximation to the PDF of possible model output and serves as an excellent characterization of the uncertainties in simulations (Hanna et al.,

2001). However, this method is more suited to deal with the uncertainty related to the continuous variables, such as input data or parameters in parameterization. The ensemble method, based on a set of different models, is an alternative approach to accounting for the range of uncertainties (Galmarini et al., 2004;Mallet and Sportisse, 2006). For example, the Air Quality Model Evaluation International Initiative (AQMEII) has been implemented in Europe and North America to investigate the model uncertainties of their regional-scale model predictions (Rao et al., 2011). To assess the model performances and uncertainties in East Asia applications, the Model Inter-Comparison Study for Asia (MICS-Asia) has been initiated in year 1998. The first Phase of MICS-Asia (MICS-Asia I) was carried out during period 1998–2002, mainly focusing on the long-range transport and depositions of sulfur in Asia (Carmichael et al., 2002). In 2003, the second phase (MICS-Asia II) was initiated and took more species related to the regional health and ecosystem protection into account, including nitrogen compounds, O_3 and aerosols. Launched in 2010, MICS-Asia III has greatly expanded its study scope by covering three individual and interrelated topics: (1) evaluate strength and weaknesses of current multi-scale air quality models and provide techniques to reduce uncertainty in Asia; (2) develop a reliable anthropogenic emission inventories in Asia and understanding uncertainty of bottom-up emission inventories in Asia; (3) provide multi-model estimates of radiative forcing and sensitivity analysis of short-lived climate pollutants.

This study addresses one component of topic 1, focusing on the three gas pollutants of NO_2, CO and NH_3. Compared with MICS-Asia II, more modeling results (fourteen different models with thirteen regional models and one global model) were brought together within the topic 1 of MICS-Asia III, run by independent modeling groups from China, Japan, Korea, United States of America and other countries/regions. The different models contain differences in their numerical approximations (time step, chemical solver, etc.) and parameterizations, which represent a sampling of uncertainties residing in the air quality modeling. However, it would be difficult to interpret the results from inter-comparison studies when the models were driven by different meteorological fields and emission inventories. Thus, in MICS-Asia III the models were constrained to be operated under the same conditions by using the common emission inventories, meteorological fields, modeling domain and horizontal resolutions. The simulations were also extended from the four months in MICS-Asia II to one-full year of 2010.

NO_2, CO and NH_3 are three important primary gas pollutants that has wide impacts on the atmospheric chemistry. As a major precursor of O_3, NO_2 plays an important role in the tropospheric O_3 chemistry, and also contributes to the rainwater acidification and the formation of secondary aerosols (Dentener and Crutzen, 1993;Evans and Jacob, 2005). CO is a colorless and toxic gas ubiquitous throughout the atmosphere which is of interest as an indirect greenhouse gas (Gillenwater, 2008) and a precursor for tropospheric O_3 (Steinfeld, 1998). Being the major sink of OH, CO also controls the atmosphere's oxidizing capacity (Levy, 1971;Novelli et al., 1998). As the only primary alkaline gas in the atmosphere, NH_3 is closely associated with the acidity of precipitations for one thing, for another it can react with sulfuric acid and nitric acid forming ammonium sulfate and ammonium nitrate which account for a large proportion of fine particulate matter (Sun et al., 2012;Sun et al., 2013). Assessing their model performances is thus important to help us better understand their environmental consequences and also help explain the model performances for their related secondary air pollutants, such as O_3 and fine particulate matter.

In previous phase of MICS-Asia, no specific evaluation and inter-comparison work has been conducted for these gases, especially for CO and NH_3. In MICS-Asia II, model performance of NO_2 was evaluated as a relevant species to O_3 (Han et al., 2008b), however such evaluations were limited to the observation sites from EANET (Acid Deposition Monitoring Network in East Asia). Model evaluations and inter-comparisons in industrialized regions of China has not been performed due to the limited number of monitoring sites in China from EANET, which hindered our understanding of the model performance in industrialized regions. More densely observations over highly industrialized regions of China, namely the North China (NCP) Plain and Pearl River Delta (PRD) regions, were first included in MICS-Asia III, allowing the model evaluations over highly industrialized regions. Meanwhile, the emission inventories of these three gases still subject to the large uncertainties (Kurokawa et al., 2013;Li et al., 2017b), which is a major source of uncertainties in air quality modeling and forecast. Evaluating these gases' emission inventories from a model perspective is also a useful way to identify the uncertainties in emission inventories (Han et al., 2008a;Noije et al., 2006;Pinder et al., 2006;Stein et al., 2014;Uno et al., 2007).

In all, this paper is aimed at evaluating the NO_2, CO and NH_3 simulations using the multi-model data from MICS-Asia III, three questions are trying to be addressed: (1) what is the performance of current CTMs in simulating the NO_2, CO and NH_3 concentrations over highly industrialized regions of China, (2) what are the potential factors responsible for the model deviations from observations and differences among models, and (3) how large are the impacts of model uncertainties on the simulations of these gases.

2 Inter-comparison frameworks

2.1 Description on the participating models and input datasets

Six different chemical transport models have participated in MICS-Asia III with their major configurations summarized in Table 1. These models included NAQPMS (Wang et al., 2001), three versions of CMAQ (Byun and Schere, 2006), WRF-Chem (Grell et al., 2005), NU-WRF (Peters-Lidard et al., 2015), NHM-Chem (Kajino et al., 2012) and GEOS-Chem (http://acmg.seas.harvard.edu/geos/). All models employed a same modeling domain (Fig. 1) with a horizontal resolution of 45km except M13 (0.5° of latitude×0.667° of longitude) and M14 (64km×64km). Detailed information on each component of these CTMs can be obtained from the companion paper Chen et al., 2019 and Tan et al., 2019.

Standard model input datasets of raw meteorological fields, emission inventory and boundary conditions were provided by MICS-Asia III for all participants. Raw meteorological fields were generated from a whole year simulations of 2010 using Weather Research and Forecasting Model (WRF) version 3.4.1 (Skamarock, 2008) with horizontal resolution of 45km and vertically 40 layers from surface to the model top (10hPa). Initial and lateral boundary conditions for meteorological simulation were generated every six hours by using the 1°×1° NCEP FNL (Final) Operational Global Analysis data (ds083.2). Real-time, global, sea surface temperature (RTG_SST_HR) analysis were used to generate and update lower boundary conditions for sea areas. Four-dimensional data assimilation nudging (Gridded FDDA & SFDDA) was performed during the simulation to increase the accuracy of WRF after the objective analysis with NCEP FNL (Final) Operational Global Analysis data (ds083.2),

NCEP ADP Global Surface Observation Weather Data (ds461.0) and NCEP ADP Global Upper Air and Surface Weather Data (ds337.0). Detailed configurations of the standard meteorological model are available in supplementary Table S1. The simulated wind speed, relative humidity and air temperature were evaluated against the observations over the NCP and PRD regions with detailed results shown in supplementary Sect. S1. In general, the standard meteorological simulations well captured the main features of meteorological conditions in the NCP and PRD regions with high correlation coefficient, small biases and low errors for all meteorological parameters (supplementary Fig.S1-S3 and Table S2).

Standard emission inventories provided by the MICS-Asia III were used by all participants. The anthropogenic emissions were provided by a newly developed anthropogenic emission inventory for Asia (MIX) which integrated five national or regional inventories, including Regional Emission inventory in Asia (REAS) inventory for Asia developed at the Japan National Institute for Environment Studies, the Multi-resolution Emission Inventory for China (MEIC) developed at Tsinghua University, the high-resolution ammonia emission inventory in China developed at Peking University, the Indian emission inventory developed at Argonne National Laboratory in the United States, and the Clean Air Policy Support System (CAPSS) Korean emission inventory developed at Konkuk University (Li et al., 2017b). Hourly biogenic emissions for the entire year of 2010 in MICS-Asia III were provided by the Model of Emissions of Gases and Aerosols from Nature version 2.04 (Guenther et al., 2006). The Global Fire Emissions Database 3 (Randerson et al., 2013) was used for biomass burning emissions. Volcanic SO_2 emissions were provided by the Asia Center for Air Pollution Research (ACAP) with a daily temporal resolution. Air and ship emissions with an annual resolution were provided by the HTAPv2 emission inventory for 2010 (Janssens-Maenhout et al., 2015). NMVOC emissions were spectated into the model-ready inputs for three chemical mechanisms: CBMZ, CB05 and SAPRC-99 and the weekly and diurnal profiles for emissions were also provided.

MICS-Asia III has provided two sets of top and lateral boundary conditions for year 2010, which were derived from the 3-hourly global CTM outputs of CHASER (Sudo et al., 2002a; Sudo et at., 2002b) and GEOS-Chem (http://acmg.seas.harvard.edu/geos/), run by Nagoya University (Japan) and the University of Tennessee (USA) respectively. GEOS-Chem was run with 2.5º×2º resolution and 47 vertical layers while CHASER model was run with 2.8º×2.8º and 32 vertical layers.

All participants were required to use the standard model input data to drive their model run so that impacts of model input data on simulations could be minimized. However, models are quite different from each other, and it is difficult to keep all the inputs the same. The majority of models have applied the standard meteorology fields, while the GEOS-Chem and RAMS-CMAQ utilized their own meteorology models. The GEOS-Chem was driven by the GEOS-5 assimilated meteorological fields from the Goddard Earth Observing System of the NASA Global Modeling Assimilation Office, and the RAMS-CMAQ was driven by meteorological fields provided by Regional Atmospheric Modeling System (RAMS) (Pielke et al., 1992). WRF-Chem utilized the same meteorology model (WRF) as the standard meteorological simulation, but two of them considered the two-way coupling effects of pollutants and meteorological fields. The meteorological configurations of these WRF-Chem models were compared to the configurations of the standard meteorological model (supplementary table S1), which shows slight differences from the standard meteorological model. The CTM part of NHM-Chem is coupled with the JMA's non-

hydrostatic meteorological model (NHM) (Saito et al., 2006), but an interface to convert a meteorological model output of WRF to a CTM input was implemented (Kajino et al., 2018). Thus, the standard meteorology field was used in the NHM-Chem simulation, too.

2.2 Data and statistical methods

All modeling groups have performed a base year simulations of 2010 and were required to submit their modeling results according to the data protocol designed in MICS-Asia III. Gridded monthly concentrations of NO_2, CO, NH_3 and ammonium (NH_4^+) in the surface layer were used in this study. Note that modeling results from M3 and NH_3 simulations from M8 were excluded due to their incredible results, thus only thirteen modeling results were used in this study.

Hourly observed concentrations of NO_2 and CO were collected over the NCP (19 stations) and PRD (13 stations) regions, obtained from the air quality network over North China (Tang et al., 2012) and the Pearl River Delta regional air quality monitoring network (PRD RAQMN), respectively. The air quality monitoring network over North China was set up by the Chinese Ecosystem Research Network (CERN), the Institute of Atmospheric Physics (IAP) and the Chinese Academy of Sciences (CAS) since 2009 within an area of 500×500 km^2 in northern China. All monitoring stations were selected and set up according to the US EPA method designations (Ji et al., 2012). The PRD RAQMN network was jointly established by the government of the Guangdong Province and the Hong Kong Special Administrative Region, consisting of 16 automatic air quality monitoring stations across the PRD region (Zhong et al., 2013). Thirteen of these stations are operated by the Environmental Monitoring Centers in the Guangdong Province which were used in this study, while the other three are located in Hong Kong (not included in this study) and are managed by the Hong Kong Environmental Protection Department. Monthly averaged observations were calculated for the comparisons with the simulated monthly surface NO_2 and CO concentrations. It should be noted that these networks measured the NO_2 concentrations using a thermal conversion method, which would overestimate the NO_2 concentrations due to the positive interference of other oxidized nitrogen compounds (Xu et al., 2013).

NH_3 observations for long-term period are indeed challenging and limited due to its strong spatial and temporal variability, quick conversion from one phase to another and also its stickiness to the observational instruments (von Bobrutzki et al., 2010). Measurements of surface NH_3 concentrations in year 2010 were not available in this study, however, one-year surface measurement of monthly NH_3 concentrations over China from September of 2015 to August of 2016 were used as a reference dataset in this study, which were obtained from the Ammonia Monitoring Network in China (AMoN-China) (Pan et al., 2018) The AMoN-China was established based on the CERN and the Regional Atmospheric Deposition Observation Network in North China Plain (Pan et al., 2012), which consists of 53 sites over the whole China and measured the monthly ambient NH_3 concentrations using the passive diffusive technique. Eleven stations located in the NCP region were used in this study. Distributions of the observation sites of NO_2, CO and NH_3 over the NCP and PRD regions as well as their total emissions in year 2010 provided by MICS-Asia III are shown in Fig. 1. Besides the surface observations, the satellite retrievals of NH_3 total columns from IASI (Infrared Atmospheric Sounding Interferometer) were also used in this study to quantitatively evaluate the modeled monthly variations of NH_3 concentrations. The ANNI-NH3-v2.1R-I retrieval product (Van Damme et al., 2017;Van

Damme et al., 2018) was used in this study which is the reanalysis version of NH_3 retrievals from IASI instruments and provides the daily morning (~9:30 am local time) NH_3 total columns from year 2008 to 2016. More detailed information and the process of satellite data are available in supplementary sect. S2.

Mean bias error (MBE), normalized mean bias (NMB), root mean square error (RMSE) and correlation coefficient (R) were calculated for the assessment of model performances. Standard deviation of the ensemble models was used to measure the ensemble spread and the impacts of model uncertainty. Coefficient of variation (hereinafter, CV), defined as the standard deviation divided by the average with larger value denoting lower consistency among models, was also used to measure the impacts of model uncertainty in a relative sense. However, by this definition, there is a tendency that lower concentrations are more likely associated with higher value of CV, thus we did not calculate the values of CV over model grids whose simulated concentrations were lower than 0.1 ppbv for NO_2 and NH_3, and 0.1 ppmv for CO, respectively. March–May, Jun–August, September–November and December–February were used to define the four seasons that are spring, summer, autumn and winter, respectively.

3 Results

3.1 Evaluating the ensemble models with observations

To facilitate comparisons, the modeling results were interpolated to the observation sites by taking the values from the grid cell where the monitoring stations located. Model evaluation metrics defined in Sect. 2.2 were then calculated to evaluate the modeling results against the observations.

3.1.1 NO_2

Figure 2 displays the comparisons between the observed and simulated annual mean NO_2 concentrations over the NCP (2a) and PRD(2b) regions with calculated model evaluation metrics summarized in Table 2. M13 is not included in the evaluation of NO_2 since it did not submitted the NO_2 concentrations. In general, the majority of models underpredicted NO_2 levels in both the NCP and PRD regions. Calculated MBE (NMB) ranges from -6.54 ppbv (-28.4%) to -2.45 (-10.6%) ppbv over the NCP region and from -9.84 ppbv (-44.0%) to -1.84 ppbv (-8.2%) over the PRD regions among these negatively-biased models. These underpredicted NO_2 concentrations are consistent with the overpredicted O_3 concentrations by these models found in the companion paper by Li et al., 2019. O_3 productions can either increase with NO_x under NO_x limited conditions or decrease under the NO_x saturated (also called volatile organic compounds (VOCs) limited) conditions (Sillman, 1999). Both the NCP and PRD regions are industrialized regions in China with high NO_x emissions (Fig. 1). Observations also showed that the NCP and PRD regions are falling into or changing into the NO_x saturated regimes (Shao et al., 2009;Jin and Holloway, 2015). Therefore, the underestimated NO_2 concentrations may contribute to the overpredicted O_3 concentrations in these two regions. More details about the O_3 predictions can be found in the companion paper by Li et al., 2019. In addition, as we mentioned in Sect.2.2, the negative biases in the simulated NO_2 concentrations can be also partly attributed to the positive

biases in the NO_2 observations. M5, M8, M9 and M11 in the NCP region and M5, M8 and M11 in the PRD region were exceptions that overpredicted NO_2 concentrations. M11 showed good performances in predicting NO_2 levels in the NCP region with smallest RMSE, while M9 significantly overestimated NO_2 with largest MBE and RMSE values. NO_2 predictions by M8 were close to the observations over the PRD region with smallest RMSE value. Meanwhile, we also found that models exhibited better NO_2 modeling skills in the NCP region than that in the PRD region with smaller bias and RMSE values.

According to the spatial correlation coefficients (Table 2), all models well reproduced the main features of the spatial variability of NO_2 concentrations in the NCP region with correlation coefficients ranging from 0.57 to 0.70. However, models failed in capturing the spatial variability of NO_2 concentrations in the PRD region with correlation coefficients only ranged from 0.00 to 0.38. Such low correlation might be attributed to the coarser model resolution (45km) that some local impacts on the NO_2 concentrations might not be well resolved in the model, and/or related to the uncertainties in emission inventories which were not well resolved in the PRD region. To investigate it, we have conducted an additional one-year simulation with finer horizontal resolutions (15km and 5km, supplementary Fig.S4) in the PRD region using the NAQPMS model. Detailed experimental settings are presented in supplementary Sect.S3. The experiment results indicate that when using the same emission inventory as the coarse-resolution simulation, the high-resolution simulation still show poor model performances in capturing the spatial variability of NO_2 concentrations in the PRD region, with calculated correlation coefficient only of 0.03 and 0.02 for 15km and 5km resolutions, respectively (supplementary Sect. S3, Fig. S5-6 and Table S3). Thus, the poor model performance in the PRD region could be more related to the coarse resolution and/or inappropriate spatial allocation of the emission inventories. These results also suggested that only increasing the resolutions of model may not help improve the model performance.

Figure 3 presents the monthly timeseries of the observed and simulated regional mean NO_2 concentrations over the NCP (3a) and PRD (3b) regions from January to December in 2010. The models well captured the monthly variations of NO_2 concentrations both in the NCP and PRD regions. According to Table 2, the correlation coefficient ranges from 0.28 to 0.96 in the NCP region and from 0.52 to 0.95 in the PRD region. M8 showed the largest overestimation among all models in summer that MBE (NMB) can reach 12.1 ppbv (75.8%) in the NCP region, which may help explain the low correlation of this model. M9 exhibited a significant overestimation in winter in the NCP region with MBE (NMB) up to 22.0 ppbv (79.3%) while much less overestimation or even underestimation (summer) in other seasons. This discrepancy may be explained by that M9 was an online coupled model which considers two-way coupling effects between the meteorology and chemistry. During the period with heavy haze, the radiation can be largely reduced by aerosol dimming effects, leading to weakened photochemistry, lowered boundary layer height and thus the increase of NO_2 concentrations. Severe haze was reported to occur in North China in January 2010, with maximum hourly $PM_{2.5}$ concentration even reached as high as ~500 $\mu g/m^3$ in urban Beijing (Gao et al., 2018). Such high aerosol loadings in atmosphere could trigger interactions between chemistry and meteorology. Interestingly, M9 did not overestimate NO_2 during winter in the PRD region. This might be related to the lower aerosol concentrations and weaker chemistry-and-meteorology coupling effects in the PRD region.

3.1.2 CO

Similar analyses were performed for modeling results of CO. All models significantly underestimated the annual mean CO concentrations both in the NCP and PRD regions (Figs. 2c-d and Table 2). Calculated MBE (NMB) ranges from -1.69 ppmv (-76.2%) to -1.16 ppmv (-52.0%) in the NCP region and from -0.67 ppmv (-69.6%) to -0.50 ppmv (-52.3%) in the PRD region (Table 2). Such large negative biases in all models were not likely to be explained by the model uncertainties, suggesting the negative biases in the CO emissions over China. This is consistent with the inversion results of Tang et al., 2013 which indicates a significant underestimation of CO emissions over the Beijing and surrounding areas in the summer of 2010. Over the latest decades, global models also reported CO underestimations in north hemisphere (Naik et al., 2013;Stein et al., 2014) and a number of global model inversion studies have been conducted to derive the optimized CO emissions. Most of these studies have reported a significant underestimation of CO emissions in their *a priori* estimates (Bergamaschi et al., 2000;Miyazaki et al., 2012;Petron et al., 2002;Petron et al., 2004). Our findings agree with these studies and indicate that more accurate CO emissions are needed in future studies. Model performances in simulating spatial variability of CO concentrations were still poor in the PRD region according to Table 2 with most models showing negative correlation coefficients.

Timeseries of the observed and simulated regional mean CO concentrations in the NCP and PRD regions are presented in Fig.3c-d. It shows that the models well reproduced the monthly variations of CO concentrations in both the NCP and PRD regions with high temporal correlation coefficient except M5 (Table 2). All models, however, underestimated CO concentrations throughout the year and showed largest underestimations in winter with MBE (NMB) by ensemble mean up to -2.1 ppmv (-64.9%) in the NCP region and -0.75 ppmv (-60.6%) in the PRD region.

3.1.3 NH_3

Figure 2e shows the comparisons of the observed and simulated annual mean NH_3 concentrations in the NCP region. Since we used the NH_3 observations from September 2015 to August 2016, negative biases are expected according to the increasing trend of atmospheric ammonia during period 2003–2016 detected by recently retrievals from the Atmospheric Infrared Sounder (AIRS) aboard NASA's Aqua satellite (Warner et al., 2016;Warner et al., 2017). Due to the interannual uncertainty, we mainly focused on the disparities among different models rather than the deviation from observations.

Large differences can be seen in simulated NH_3 concentrations from different models. M14 simulated very low concentrations and exhibited the largest negative biases with MBE (NMB) of -12.2 ppbv (-66.3%), which may be related to the higher conversion rate of NH_3 to NH_4^+ in M14 (discussed in later part of this section). On the contrary, M9 provided much higher NH_3 concentrations than other models with MBE (NMB) up to 21.8 ppbv (118.7%). For the CMAQ models, M1 and M2 exhibited higher NH_3 concentrations and larger spatial variability compared to other CMAQ models. Such discrepancy may be explained by that M1 and M2 are two model runs using CMAQ v5.0.2. The bi-directional exchange of NH_3 has been integrated into CMAQ from version 5.0. This module can simulate the emitted and deposited processes of NH_3 between

atmosphere and the surfaces, allowing the additional NH_3 emissions to the atmosphere (US EPA Office of Research and Development).

As can be seen in Table 2, the observed spatial variations of NH_3 over the NCP region can be well reproduced by all models (R = 0.57-0.71), indicating that the spatial variations of current NH_3 emissions over the NCP region are well represented in emission inventories. However, all models failed to capture the observed monthly variations of NH_3 concentrations with most models mismatching the observed NH_3 peak (July) and showing negative correlation coefficients. M10 and M13 are exceptions showing good temporal correlations of 0.64 and 0.65, respectively (Fig. 3e and Table 2). This is quite different from the model behavior in simulating the monthly variations of NO_2 and CO concentrations. As seen in Fig. 3e, the observation showed the peak concentrations of NH_3 in summer months and lower concentrations in autumn and winter, which is consistent with the previous NH_3 observations in the NCP region (Shen et al., 2011;Xu et al., 2016;Meng et al., 2011). Newly derived satellite-measured NH_3 at 918 hPa averaged between September 2002 and August 2015 also demonstrated higher concentrations in spring and summer and lower concentrations in autumn and winter (Warner et al., 2016). However, all models predicted a peak concentration in November except M10 in August in and M13 in June. We also used the satellite retrievals of NH_3 total columns from IASI to further evaluate the modeled monthly variations of NH_3 concentrations, since evaluating the model results using observations from different years may be inappropriate due to the emission change of NH_3. Comparisons of the surface NH_3 observations from AMoN-China and NH_3 total columns form IASI (supplementary Fig.S7) suggest that the IASI measurement can well represent the monthly variations of surface NH_3 concentrations, which can be used to qualitatively evaluate the modeled monthly variations of surface NH_3 concentrations. The monthly time series of the regional mean NH_3 total columns over the NCP region from January, 2008 to December, 2016 are shown in supplementary Fig. S8, which shows similar monthly variations to the surface NH_3 observations with highest value in July and confirms the poor model performances in reproducing the monthly variations of NH_3 concentrations. The IASI measurement also indicates that the interannual variability of monthly variations of NH_3 concentrations over the NCP region was small from year 2008 to 2016, which suggest that using observations from different years could still provide valuable clues for verifying the modeled monthly variations.

The simulated monthly variations of NH_3 concentrations were closely related to the monthly variations of the NH_3 emissions. Most models predicted three peak values of NH_3 concentrations in June, August and November but exhibited a significant decrease in July, which was in good agreement with the peaks and drops of the NH_3 emission rates in these months (Fig.4). The strong relationship between the simulated NH_3 concentrations and the emission rates suggests that the poor model performance in reproducing the monthly variations of NH_3 concentrations is probably related to the uncertainties in the monthly variations of NH_3 emissions. This is consistent with the recent bottom-up and top-down estimates of agriculture ammonia emissions in China by (Zhang et al., 2018), which shows more distinct seasonality of Chinese NH_3 emissions.

It is worth noting that there are also important uncertainties in the models beyond emission uncertainty. In order to investigate this issue, we have analyzed the impact of gas-aerosol partitioning of NH_3 on the simulations of NH_3 concentrations. Figure 5 shows the timeseries of the simulated total ammonium ($NH_x = NH_3 + NH_4^+$) in the atmosphere along with the ratio

of gaseous NH_3 to the total ammonium. M10 is excluded in Fig.5 since the GOCART model does not predict NH_4^+ concentrations. As a result, the emitted NH_3 would be only presented as the gas phase in M10, leading to higher NH_3 predictions. This may also help explain the different monthly variations of NH_3 concentrations seen in M10. Without the considerations of NH_4^+, the monthly variations of NH_3 concentrations in M10 were more consistent with the monthly variations of NH_3 emissions, which highlighted the importance of gas-aerosol partitioning of NH_3 on the predictions of monthly variations of NH_3 concentrations. As seen in fig.5, there are large discrepancy in the simulated gas-aerosol partitioning of NH_3 from different models. M7 and M9 showed higher NH_3/NH_x ratio than other models, which means that these two models tended to retain the NH_3 in the gas phase and thus predicted higher NH_3 concentrations than other models. For example, M7 predicted comparable magnitude of total ammonium with most models, while gas NH_3 concentration in M7 accounted for more than 60% of total ammonium in summer and even 90% in winter. The lower conversion rate of NH_3 to NH_4^+ in M9 may be related to the gas phase chemistry used in the model. M9 used the RADM2 mechanism which gives lower reaction rates of oxidation of SO_2 and NO_2 by the OH radical as compiled by Tan et al., 2019, leading to lower productions of acid and thus lower conversion rate of NH_3 to NH_4^+. In case of M7, the hydrolysis of N_2O_5 was not considered in M7, which leads to a lower tendency in the prediction of NO_3^- (Chen et al., 2019) and partly explains the higher NH_3 predictions of M7. On the contrary, M14 showed a much lower NH_3/NH_x ratio than most models, which would be related to its higher production rates of sulfate than other models as seen in Chen et al., 2019. In terms of monthly variations, most models predicted lower NH_3/NH_x ratio in summer than that in other seasons, suggesting the higher conversion rates of NH_3 from gas phase to aerosol phase in summer. This would be related to the higher yield of ammonium sulfate due to the enhanced photochemical oxidation activity in summer. However, different from the modeling results, the NH_3 and NH_4^+observations over the NCP region indicated a lower NH_3/NH_x ratio with higher ammonium concentrations in autumn and winter (Shen et al., 2011;Xu et al., 2016). Although observed NH_4^+ was largest in summer at a rural site in Beijing, observed NH_3/NH_x ratio was still highest in summer according to observations from Meng et al., 2011. These results indicate that there would be large uncertainties in the modeling of seasonal variations of the gas-aerosol partitioning of NH_3 over the NCP region. The formation of NH_4^+ mainly depends on the acid gas concentrations, temperature, water availability (Khoder, 2002) and the flux rates of NH_3 (Nemitz et al., 2001). Compared with spring and summer, the lower temperature and higher SO_2 and NO_x emissions should favor the gas-to-particle phase conversion of NH_3 and lead to higher NH_4^+ concentrations. This contrast indicates that some reaction pathways of acid productions (H_2SO_4 or HNO_3) may be missing in current models, such as aqueous-phase and heterogeneous chemistry (Cheng et al., 2016;Wang et al., 2016;Zheng et al., 2015). Such uncertainty may be another important factor contributing to the poor model performances in reproducing the monthly variations of NH_3 concentrations over the NCP region.

3.2 Quantifying the impacts of model uncertainty

In this section, we further investigate the discrepancies among the different models to quantify the impacts of model uncertainty on the simulations of these gases. As we mentioned in Sect. 2, most of these models employed common

meteorology fields and emission inventories over China under the same modeling domain and horizontal resolutions, which composed an appropriate set for the investigations of model uncertainties.

Figures 6–8 present the simulated annual mean concentrations of NO_2, CO and NH_3 from different models. The spatial distributions of the simulated NO_2, CO and NH_3 concentrations from different models agreed well with each other, similar to the spatial distributions of their emissions (Fig. 1). High NO_2 concentrations were mainly located in the north and central-east China, and several hot-spots of NO_2 were also detected in the northeast China and the PRD region. M5, M8, M9, and M11 predicted higher NO_2 concentrations than other models especially for M8 which also predicted very high NO_2 levels over southeast China. Similar to NO_2, high CO concentrations were generally located over the north and central-east China as well as the east of Sichuan basin. M8, M9 and M11 predicted higher CO concentrations than other models as well. In terms of NH_3, although most models shared similar spatial patterns of NH_3 simulations, the simulated NH_3 concentrations varied largely from different models. High NH_3 concentrations were mainly located over the north China and India peninsula, which was in accordance with the distribution of agricultural activity intensity over East Asia. Among these models, M9 and M10 produced much higher NH_3 concentrations over East Asia while M4, M5, M6, M13 and M14 produced much lower concentrations.

The impacts of model uncertainty on the simulations of NH_3 (9a), CO (9b) and NO_2 (9c) were then quantified in Fig.9, denoted by the spatial distributions of the standard deviation (ensemble spread) and the corresponding distributions of CV on the annual and seasonal basis. Note that M13 and M14 are excluded in the calculation of ensemble spread and CV to reduce the influences of the meteorological input data and horizontal resolutions. It seems that the impacts of model uncertainty increase with the reactivity of gases. NH_3 simulations were affected most by the model uncertainty, while CO suffered least from the uncertainty in models.

The ensemble spread of NH_3 simulations exhibited a strong spatial variability with higher values mainly located in the NCP region. Standard deviation of the annual mean NH_3 concentrations can be over 20 ppbv in Henan province and 15 ppbv in the south of Hebei province, which is about 60–80% and 40–60% of the ensemble mean respectively according to the CV distribution. As we mentioned in Sect. 3.1.3, these large modeling differences can be partly explained by the differences in the bi-directional exchange and gas-aerosol partitioning of NH_3 in different models. A strong seasonal pattern was also found in the differences of NH_3 simulations over the NCP region. The ensemble spread was smallest in spring while largest in autumn, up to 25 ppbv in most areas of the NCP region. However, in the relative sense, the modeling differences were larger in summer and winter while less in spring and autumn. The southeast China shared a similar magnitude of the ensemble spread (2–5 ppbv) and showed weaker seasonal variability. However, the modeling differences in the relative sense were larger than that in the NCP region with CV over 1.0 in all seasons except that in Summer. This can be due to that the simulated concentrations may be more influenced by the model processes over the areas with low emissions, while more constrained by the emissions over high emission rate areas.

CO was least affected by the model uncertainty among the three gases which is consistent with its weaker chemical activity and longer lifetime in the atmosphere. The ensemble spread of annual mean CO concentration was about 0.05–0.2 ppmv in the east China, only about 20%–30% of the ensemble mean. Meanwhile, CO modeling differences was more

uniformly distributed in east China with CV less than 0.3 over most areas of east China. However, large modeling differences were visible over Myanmar during spring when there were high CO emissions from biomass burning. Model differences turned to be larger during winter in the NCP region with ensemble spread and CV about 0.3–0.5 ppmv and 0.3–0.4, respectively.

NO_2 was mediumly affected by the model uncertainty among the three gases. Ensemble spread of annual mean NO_2 concentration was 5–7.5 ppbv in the NCP region and 2.5–5 ppbv in the southeast China, which accounted for about 20%–30% of the ensemble mean in the former but more than 70% in the latter. The ensemble spread was largest in winter which was over 10 ppbv in the NCP region (30%–40%) and 5–7.5 ppbv in southeast China (over 70%). Similar to NH_3, southeast China exhibited more modeling differences than the NCP region in relative sense with CV higher than 0.7 in most areas of southeast China.

4 Summary

In this study, thirteen modeling results of surface NO_2, CO and NH_3 concentrations from MICS-Asia III were compared with each other and evaluated against the observations over the NCP and PRD regions. Three questions are trying to be addressed which are related to the performance of current CTMs in simulating the NO_2, CO and NH_3 concentrations over the highly industrialized regions of China, potential factors responsible for the model deviations from observations and differences among models, and the impacts of model uncertainty on the simulations of these gases.

Most models showed underestimations of NO_2 concentrations in the NCP and PRD regions, which could be an important potential factor contributing to the overpredicted O_3 concentrations in these regions. According to Xu et al., 2013, such underestimations would also be related to the positive biases in the NO_2 observations. The models showed better NO_2 model performance in the NCP region than that in the PRD region with smaller biases and RMSE. Most models well reproduced the observed temporal and spatial patterns of NO_2 concentrations in the NCP region, while relatively poor model performance was found in the PRD region in terms of the spatial variations of NO_2 concentrations. A sensitivity test with finer horizontal resolutions has been conducted to investigate the potential reasons for the poor model performance in the PRD region. The results shows that only increasing the model resolution cannot improve the model performance in the PRD region, which suggest that the poor model performance in the PRD region would be more related to the coarse resolution and/or inappropriate spatial allocations of the emission inventories in the PRD regions. All models significantly underestimated the CO concentrations in the NCP and PRD regions throughout the year. Such large underestimations of all models are not likely to be fully explained by the model uncertainty, which suggests that CO emissions may be underestimated in current emission inventories. More accurate estimate of CO emissions is thus needed for year 2010. Underestimations of CO emissions may be alleviated in recent years due to the decreasing trends of the Chinese CO emissions in recent years(Jiang et al., 2017;Zhong et al., 2017;Sun et al., 2018;Muller et al., 2018;Zheng et al., 2018;Zheng et al., 2019). The inversion results of Zheng et al., 2018 also agree well with the MEIC inventory for CO emissions in China from 2013 to 2015. However uncertainties still exist in the CO emissions for recent years, according to previous studies, the estimated CO emissions in China ranges from 134–202

Tg/yr in year 2013 (Jiang et al., 2017;Zhong et al., 2017;Sun et al., 2018;Muller et al., 2018;Zheng et al., 2018;Zheng et al., 2019). Zhao et al., 2017 also suggested a -29%–40% uncertainty of CO emissions from the industrial sector in year 2012. For NH_3 simulations, in contrast to the good skills in the monthly variations of NO_2 and CO concentrations, all models failed to reproduce the observed monthly variations of NH_3 concentrations in the NCP region, as shown by both the surface and satellite measurements. Most models mismatched the observed peak and showed negative correlation coefficient with observations, which may be closely related to the uncertainty in the monthly variations of NH_3 emissions and also the uncertainty in the gas-aerosol partitioning of NH_3.

Several potential factors were found to be responsible for the model deviation and differences, including the emission inventories, chemistry-and-meteorology coupling effects, bi-directional exchange of NH_3 and the NH_3 gas-aerosol partitioning, which would be important aspects with respect to the model improvements in future. Previous studies also suggest that the nitrous acid (HONO) chemistry plays an important role in the atmospheric nitrogen chemistry, which influences the simulations of NO_2 and NH_3 (Fu et al., 2019;Zhang et al., 2017;Zhang et al., 2016). Heterogeneous conversion from NO_2 to HONO ($2NO_{2(g)} + H_2O_{(l)} \rightarrow HONO_{(l)} + HNO_{3(l)}$) is one of the dominant sources of HONO in the atmosphere, which has been considered in most models of MICS-Asia III, including CMAQ since version 4.7, NAQPMS, NHM-Chem and GEOS-Chem. However, some other important sources of HONO may still be underestimated by models in MICS-Asia III. For example, Fu et al., 2019 suggested that the high relative humidity and strong light could enhance the heterogeneous reaction of NO_2 , and the photolysis of total nitrate were also important sources of HONO. These sources has not been included in the models of MICS-Asia III, which would lead to the deviations from observations. The inter-comparisons of the ensemble models quantified the impacts of model uncertainty on the simulations of these gases, which shows that the impacts of model uncertainty increases with the reactivity of these gases. Models contained more uncertainties in the prediction of NH_3 than the other two gases. Based on these findings, some recommendations are made for future studies:

1) More accurate estimation of CO and NH_3 emissions are needed in future studies. Both bottom-up and top-down method (inversion technique) can help address this problem. The inversion of NH_3 emissions would be more complicated than the inversion of CO emissions due to the larger uncertainties in modeling the atmospheric processes of NH_3. Nevertheless, it could still provide valuable clues for verifying the bottom-up emission inventories (Zhang et al., 2009) if the models were well validated. In addition, by using the ground or satellite measurements, the top-down methods could also give valuable information on the spatial and temporal patterns of NH_3 emissions, for example the inversions studies by Paulot et al., 2014 and Zhang et al., 2018. However, more attention should be paid to the validations of model before the inversion estimation of NH_3 emissions. How to represent the model uncertainties in the current framework of emission inversion is also an important aspect in future studies. Things could be better for CO considering its small and weakly spatial-dependent model uncertainties.

2) For some highly active and/or short-lived primary pollutants, like NH_3, model uncertainty can also take a great part in the forecast uncertainty. Emission uncertainty alone may not be sufficient to explain the forecast uncertainty and may cause underdispersive, and overconfident forecasts. Future studies are needed in how to better represent the model uncertainties in

the model predictions to obtain a better forecast skill. Such model uncertainties also emphasize the need to validate the individual model before using its results to make important policy recommendation.

3) Gas-aerosol partition of NH_3 is shown to be an important source of uncertainties in NH_3 simulation. The formation of NH_4^+ particles is mainly limited by the availability of H_2SO_4 and HNO_3 under ammonia-rich conditions, which involves complex chemical reactions, including gas-phase, aqueous-phase and heterogeneous chemistry (Cheng et al., 2016;Wang et al., 2016;Zheng et al., 2015). These processes are needed to be verified and incorporated into models to better represent the chemistry in the atmosphere.

4) The gas chemistry mechanisms used in this study are SAPRC 99, CB05, CBMZ, RACM and RADM2, and some of them have an updated version such as CB06 and SPARC 07. Our conclusions may not be applicable to these newer versions of mechanisms and thus more comparisons studies can be performed to understand the differences in these new mechanisms.

Competing interests

The authors declare that they have no conflict of interest.

Author contribution

X.T., J.Z., Z.F.W and G.C. conducted the design of this study. J.F., X.W., S.I., K.Y., T.N., H.L., C.K., C.L., L.C., M.Z., Z.T., J.L., M.K., H.L., B.G. contributed to the modelling data. Z.W. performed the simulations of standard meteorological field. M.L. and Q.W. provided the emission data. K.S. provided the CHASER output for boundary conditions. Y.W., Y.P., G.T. provided the observation data. L.K. and X.T. performed the analysis and prepared the manuscript with contributions from all-authors.

Acknowledgements

This study was supported by the National Natural Science Foundation (Grant Nos. 91644216 & 41620104008), the National Key R&D Program (Grant Nos. 2018YFC0213503) and Guangdong Provincial Science and Technology Development Special Fund (No.2017B020216007). Yuepeng Pan acknowledges the National Key Research and Development Program of China (Grants 2017YFC0210100, 2016YFC0201802) and the National Natural Science Foundation of China (Grant 41405144) for financial support. We are indebted to the staff who collected the samples at the AMoN-China sites during the study period.

References

Anenberg, S. C., Horowitz, L. W., Tong, D. Q., and West, J. J.: An Estimate of the Global Burden of Anthropogenic Ozone and Fine Particulate Matter on Premature Human Mortality Using Atmospheric Modeling, Environ. Health Perspect., 118, 1189-1195, 10.1289/ehp.0901220, 2010.

Bergamaschi, P., Hein, R., Heimann, M., and Crutzen, P. J.: Inverse modeling of the global CO cycle 1. Inversion of CO mixing ratios, J. Geophys. Res.-Atmos., 105, 1909-1927, 10.1029/1999jd900818, 2000.

Byun, D., and Schere, K. L.: Review of the governing equations, computational algorithms, and other components of the models-3 Community Multiscale Air Quality (CMAQ) modeling system, Appl. Mech. Rev., 59, 51-77, 10.1115/1.2128636, 2006.

Carmichael, G., Sakurai, T., Streets, D., Hozumi, Y., Ueda, H., Park, S., Fung, C., Han, Z., Kajino, M., and Engardt, M.: MICS-Asia II: The model intercomparison study for Asia Phase II methodology and overview of findings, Atmos. Environ., 42, 3468-3490, 10.1016/j.atmosenv.2007.04.007, 2008.

Carmichael, G. R., Calori, G., Hayami, H., Uno, I., Cho, S. Y., Engardt, M., Kim, S. B., Ichikawa, Y., Ikeda, Y., Woo, J. H., Ueda, H., and Amann, M.: The MICS-Asia study: model intercomparison of long-range transport and sulfur deposition in East Asia, Atmos. Environ., 36, 175-199, 10.1016/s1352-2310(01)00448-4, 2002.

Chen, L., Gao, Y., Zhang, M., Fu, J. S., Zhu, J., Liao, H., Li, J., Huang, K., Ge, B., Wang, X., Lam, Y. F., Lin, C. Y., Itahashi, S., Nagashima, T., Kajino, M., Yamaji, K., Wang, Z., and Kurokawa, J. I.: MICS-Asia III: Multi-model comparison and evaluation of aerosol over East Asia, Atmos. Chem. Phys. Discuss., 2019, 1-54, 10.5194/acp-2018-1346, 2019.

Cheng, Y. F., Zheng, G. J., Wei, C., Mu, Q., Zheng, B., Wang, Z. B., Gao, M., Zhang, Q., He, K. B., Carmichael, G., Poschl, U., and Su, H.: Reactive nitrogen chemistry in aerosol water as a source of sulfate during haze events in China, Sci. Adv., 2, 11, 10.1126/sciadv.1601530, 2016.

Dabberdt, W. F., and Miller, E.: Uncertainty, ensembles and air quality dispersion modeling: applications and challenges, Atmos. Environ., 34, 4667-4673, 10.1016/s1352-2310(00)00141-2, 2000.

Dentener, F. J., and Crutzen, P. J.: REACTION OF N2O5 ON TROPOSPHERIC AEROSOLS - IMPACT ON THE GLOBAL DISTRIBUTIONS OF NOX, O3, AND OH, J. Geophys. Res.-Atmos., 98, 7149-7163, 10.1029/92jd02979, 1993.

Evans, M. J., and Jacob, D. J.: Impact of new laboratory studies of N2O5 hydrolysis on global model budgets of tropospheric nitrogen oxides, ozone, and OH, Geophys. Res. Lett., 32, 4, 10.1029/2005gl022469, 2005.

Fine, J., Vuilleumier, L., Reynolds, S., Roth, P., and Brown, N.: Evaluating uncertainties in regional photochemicalair quality modeling, Annu. Rev. Environ. Resour., 28, 59-106, 10.1146/annurev.energy.28.011503.163508, 2003.

Fu, X., Wang, T., Zhang, L., Li, Q. Y., Wang, Z., Xia, M., Yun, H., Wang, W. H., Yu, C., Yue, D. L., Zhou, Y., Zheng, J. Y., and Han, R.: The significant contribution of HONO to secondary pollutants during a severe winter pollution event in southern China, Atmos. Chem. Phys., 19, 1-14, 10.5194/acp-19-1-2019, 2019.

Galmarini, S., Bianconi, R., Klug, W., Mikkelsen, T., Addis, R., Andronopoulos, S., Astrup, P., Baklanov, A., Bartniki, J., Bartzis, J. C., Bellasio, R., Bompay, F., Buckley, R., Bouzom, M., Champion, H., D'Amours, R., Davakis, E., Eleveld, H., Geertsema, G. T., Glaab, H., Kollax, M., Ilvonen, M., Manning, A., Pechinger, U., Persson, C., Polreich, E., Potemski, S., Prodanova, M., Saltbones, J., Slaper, H., Sofiev, M. A., Syrakov, D., Sørensen, J. H., Auwera, L. V. d., Valkama, I., and Zelazny, R.: Ensemble dispersion forecasting—Part I: concept, approach and indicators, Atmos. Environ., 38, 4607-4617, https://doi.org/10.1016/j.atmosenv.2004.05.030, 2004.

Gao, D. F., Stockwell, W. R., and Milford, J. B.: Global uncertainty analysis of a regional-scale gas-phase chemical mechanism, J. Geophys. Res.-Atmos., 101, 9107-9119, 10.1029/96jd00060, 1996.

Gao, M., Han, Z. W., Liu, Z. R., Li, M., Xin, J. Y., Tao, Z. N., Li, J. W., Kang, J. E., Huang, K., Dong, X. Y., Zhuang, B. L., Li, S., Ge, B. Z., Wu, Q. Z., Cheng, Y. F., Wang, Y. S., Lee, H. J., Kim, C. H., Fu, J. S. S., Wang, T. J., Chin, M. A., Woo, J. H., Zhang, Q., Wang, Z. F., and Carmichael, G. R.: Air quality and climate change, Topic 3 of the Model Inter-Comparison Study for Asia Phase III (MICS-Asia III) - Part 1: Overview and model evaluation, Atmos. Chem. Phys., 18, 4859-4884, 10.5194/acp-18-4859-2018, 2018.

Gillenwater, M.: Forgotten carbon: indirect CO2 in greenhouse gas emission inventories, Environ. Sci. Policy, 11, 195-203, 10.1016/j.envsci.2007.09.001, 2008.

Grell, G. A., Peckham, S. E., Schmitz, R., McKeen, S. A., Frost, G., Skamarock, W. C., and Eder, B.: Fully coupled "online" chemistry within the WRF model, Atmos. Environ., 39, 6957-6975, 10.1016/j.atmosenv.2005.04.027, 2005.

Guenther, A., Karl, T., Harley, P., Wiedinmyer, C., Palmer, P. I., and Geron, C.: Estimates of global terrestrial isoprene emissions using MEGAN (Model of Emissions of Gases and Aerosols from Nature), Atmos. Chem. Phys., 6, 3181-3210, 2006.

Han, K. M., Song, C. H., Ahn, H. J., Park, R. S., Woo, J. H., Lee, C. K., Richter, A., Burrows, J. P., Kim, J. Y., and Hong, J. H.: Investigation of NO_x emissions and NO_x-related chemistry in East Asia using CMAQ-predicted and GOME-derived NO2 columns, Atmos. Chem. Phys., 9, 17297-17341, 2008a.

Han, Z., Sakurai, T., Ueda, H., Carmichael, G., Streets, D., Hayami, H., Wang, Z., Holloway, T., Engardt, M., and Hozumi, Y.: MICS-Asia II: Model intercomparison and evaluation of ozone and relevant species, Atmos. Environ., 42, 3491-3509, 10.1016/j.atmosenv.2007.07.031, 2008b.

Janssens-Maenhout, G., Crippa, M., Guizzardi, D., Dentener, F., Muntean, M., Pouliot, G., Keating, T., Zhang, Q., Kurokawa, J., Wankmuller, R., van der Gon, H. D., Kuenen, J. J. P., Klimont, Z., Frost, G., Darras, S., Koffi, B., and Li, M.: HTAP_v2.2: a mosaic of regional and global emission grid maps for 2008 and 2010 to study hemispheric transport of air pollution, Atmos. Chem. Phys., 15, 11411-11432, 10.5194/acp-15-11411-2015, 2015.

Ji, D. S., Wang, Y. S., Wang, L. L., Chen, L. F., Hu, B., Tang, G. Q., Xin, J. Y., Song, T., Wen, T. X., Sun, Y., Pan, Y. P., and Liu, Z. R.: Analysis of heavy pollution episodes in selected cities of northern China, Atmos. Environ., 50, 338-348, 10.1016/j.atmosenv.2011.11.053, 2012.

554 Jiang, Z., Worden, J. R., Worden, H., Deeter, M., Jones, D. B. A., Arellano, A. F., and Henze, D. K.: A 15-year record of CO
555 emissions constrained by MOPITT CO observations, Atmos. Chem. Phys., 17, 4565-4583, 10.5194/acp-17-4565-2017,
556 2017.
557 Jin, X. M., and Holloway, T.: Spatial and temporal variability of ozone sensitivity over China observed from the Ozone
558 Monitoring Instrument, J. Geophys. Res.-Atmos., 120, 7229-7246, 10.1002/2015jd023250, 2015.
559 Kajino, M., Inomata, Y., Sato, K., Ueda, H., Han, Z., An, J., Katata, G., Deushi, M., Maki, T., Oshima, N., Kurokawa, J.,
560 Ohara, T., Takami, A., and Hatakeyama, S.: Development of the RAQM2 aerosol chemical transport model and
561 predictions of the Northeast Asian aerosol mass, size, chemistry, and mixing type, Atmos. Chem. Phys., 12, 11833-11856,
562 10.5194/acp-12-11833-2012, 2012.
563 Kajino, M., Deushi, M., Sekiyama, T. T., Oshima, N., Yumimoto, K., Tanaka, T. Y., Ching, J., Hashimoto, A., Yamamoto, T.,
564 Ikegami, M., Kamada, A., Miyashita, M., Inomata, Y., Shima, S. I., Adachi, K., Zaizen, Y., Igarashi, Y., Ueda, H., Maki,
565 T., and Mikami, M.: NHM-Chem, the Japan MeteorologicalAgency's regional meteorology – chemistry model (v1.0):
566 model description and aerosol representations, Geosci. Model Dev. Discuss., 2018, 1-45, 10.5194/gmd-2018-128, 2018.
567 Khoder, M. I.: Atmospheric conversion of sulfur dioxide to particulate sulfate and nitrogen dioxide to particulate nitrate and
568 gaseous nitric acid in an urban area, Chemosphere, 49, 675-684, 10.1016/s0045-6535(02)00391-0, 2002.
569 Kurokawa, J., Ohara, T., Morikawa, T., Hanayama, S., Janssens-Maenhout, G., Fukui, T., Kawashima, K., and Akimoto, H.:
570 Emissions of air pollutants and greenhouse gases over Asian regions during 2000-2008: Regional Emission inventory in
571 ASia (REAS) version 2, Atmos. Chem. Phys., 13, 11019-11058, 10.5194/acp-13-11019-2013, 2013.
572 Lelieveld, J., Evans, J. S., Fnais, M., Giannadaki, D., and Pozzer, A.: The contribution of outdoor air pollution sources to
573 premature mortality on a global scale, Nature, 525, 367-+, 10.1038/nature15371, 2015.
574 Levy, H.: NORMAL ATMOSPHERE - LARGE RADICAL AND FORMALDEHYDE CONCENTRATIONS PREDICTED,
575 Science, 173, 141-&, 10.1126/science.173.3992.141, 1971.
576 Li, J., Du, H. Y., Wang, Z. F., Sun, Y. L., Yang, W. Y., Li, J. J., Tang, X., and Fu, P. Q.: Rapid formation of a severe regional
577 winter haze episode over a mega-city cluster on the North China Plain, Environ. Pollut., 223, 605-615,
578 10.1016/j.envpol.2017.01.063, 2017a.
579 Li, J., Nagashima, T., Kong, L., Ge, B., Yamaji, K., Fu, J. S., Wang, X., Fan, Q., Itahashi, S., Lee, H. J., Kim, C. H., Lin, C.
580 Y., Zhang, M., Tao, Z., Kajino, M., Liao, H., Li, M., Woo, J. H., Kurokawa, J. I., Wu, Q., Akimoto, H., Carmichael, G.
581 R., and Wang, Z.: Model evaluation and inter-comparison of surface-level ozone and relevant species in East Asia in the
582 context of MICS-Asia phase III Part I: overview, Atmos. Chem. Phys. Discuss., 2019, 1-56, 10.5194/acp-2018-1283,
583 2019.
584 Li, M., Zhang, Q., Kurokawa, J. I., Woo, J. H., He, K., Lu, Z., Ohara, T., Song, Y., Streets, D. G., Carmichael, G. R., Cheng,
585 Y., Hong, C., Huo, H., Jiang, X., Kang, S., Liu, F., Su, H., and Zheng, B.: MIX: a mosaic Asian anthropogenic emission
586 inventory under the international collaboration framework of the MICS-Asia and HTAP, Atmos. Chem. Phys., 17, 935-
587 963, 10.5194/acp-17-935-2017, 2017b.

588 Lu, M. M., Tang, X., Wang, Z. F., Gbaguidi, A., Liang, S. W., Hu, K., Wu, L., Wu, H. J., Huang, Z., and Shen, L. J.: Source
589 tagging modeling study of heavy haze episodes under complex regional transport processes over Wuhan megacity,
590 Central China, Environ. Pollut., 231, 612-621, 10.1016/j.envpol.2017.08.046, 2017.
591 Ma, C. Q., Wang, T. J., Mizzi, A. P., Anderson, J. L., Zhuang, B. L., Xie, M., and Wu, R. S.: Multiconstituent Data Assimilation
592 With WRF-Chem/DART: Potential for Adjusting Anthropogenic Emissions and Improving Air Quality Forecasts Over
593 Eastern China, J. Geophys. Res.-Atmos., 124, 7393-7412, 10.1029/2019jd030421, 2019.
594 Mallet, V., and Sportisse, B.: Uncertainty in a chemistry-transport model due to physical parameterizations and numerical
595 approximations: An ensemble approach applied to ozone modeling, J. Geophys. Res.-Atmos., 111, 15,
596 10.1029/2005jd006149, 2006.
597 Meng, Z. Y., Lin, W. L., Jiang, X. M., Yan, P., Wang, Y., Zhang, Y. M., Jia, X. F., and Yu, X. L.: Characteristics of atmospheric
598 ammonia over Beijing, China, Atmos. Chem. Phys., 11, 6139-6151, 10.5194/acp-11-6139-2011, 2011.
599 Miyazaki, K., Eskes, H. J., Sudo, K., Takigawa, M., Weele, M. V., and Boersma, K. F.: Simultaneous assimilation of satellite
600 NO2, O3, CO, and HNO3 data for the analysis of tropospheric chemical composition and emissions, Atmos. Chem. Phys.
601 & Discussions, 264, 1017-1023, 2012.
602 Muller, J. F., Stavrakou, T., Bauwens, M., George, M., Hurtmans, D., Coheur, P. F., Clerbaux, C., and Sweeney, C.: Top-
603 Down CO Emissions Based On IASI Observations and Hemispheric Constraints on OH Levels, Geophys. Res. Lett., 45,
604 1621-1629, 10.1002/2017gl076697, 2018.
605 Naik, V., Voulgarakis, A., Fiore, A. M., Horowitz, L. W., Lamarque, J. F., Lin, M., Prather, M. J., Young, P. J., Bergmann,
606 D., Cameron-Smith, P. J., Cionni, I., Collins, W. J., Dalsoren, S. B., Doherty, R., Eyring, V., Faluvegi, G., Folberth, G.
607 A., Josse, B., Lee, Y. H., MacKenzie, I. A., Nagashima, T., van Noije, T. P. C., Plummer, D. A., Righi, M., Rumbold, S.
608 T., Skeie, R., Shindell, D. T., Stevenson, D. S., Strode, S., Sudo, K., Szopa, S., and Zeng, G.: Preindustrial to present-
609 day changes in tropospheric hydroxyl radical and methane lifetime from the Atmospheric Chemistry and Climate Model
610 Intercomparison Project (ACCMIP), Atmos. Chem. Phys., 13, 5277-5298, 10.5194/acp-13-5277-2013, 2013.
611 Nemitz, E., Milford, C., and Sutton, M. A.: A two-layer canopy compensation point model for describing bi-directional
612 biosphere-atmosphere exchange of ammonia, Q. J. R. Meteorol. Soc., 127, 815-833, 10.1256/smsqj.57305, 2001.
613 Noije, T. P. C. V., Eskes, H. J., Dentener, F. J., Stevenson, D. S., Ellingsen, K., Schultz, M. G., Wild, O., Amann, M., Atherton,
614 C. S., and Bergmann, D. J.: Multi-model ensemble simulations of tropospheric NO_2 compared with GOME retrievals for
615 the year 2000, Atmos. Chem. Phys., 6, 2943-2979, 2006.
616 Novelli, P. C., Masarie, K. A., and Lang, P. M.: Distributions and recent changes of carbon monoxide in the lower troposphere,
617 J. Geophys. Res.-Atmos., 103, 19015-19033, 10.1029/98jd01366, 1998.
618 Pan, Y., Tian, S., Zhao, Y., Zhang, L., Zhu, X., Gao, J., Huang, W., Zhou, Y., Song, Y., Zhang, Q., and Wang, Y.: Identifying
619 ammonia hotspots in China using a national observation network, Environ. Sci. Technol., 52, 3926-3934,
620 10.1021/acs.est.7b05235, 2018.

621 Pan, Y. P., Wang, Y. S., Tang, G. Q., and Wu, D.: Wet and dry deposition of atmospheric nitrogen at ten sites in Northern
622 China, Atmos. Chem. Phys., 12, 6515-6535, 10.5194/acp-12-6515-2012, 2012.
623 Paulot, F., Jacob, D. J., Pinder, R. W., Bash, J. O., Travis, K., and Henze, D. K.: Ammonia emissions in the United States,
624 European Union, and China derived by high-resolution inversion of ammonium wet deposition data: Interpretation with
625 a new agricultural emissions inventory (MASAGE_NH3), J. Geophys. Res.-Atmos., 119, 4343-4364,
626 10.1002/2013jd021130, 2014.
627 Peters-Lidard, C. D., Kemp, E. M., Matsui, T., Santanello, J. A., Kumar, S. V., Jacob, J. P., Clune, T., Tao, W. K., Chin, M.,
628 Hou, A., Case, J. L., Kim, D., Kim, K. M., Lau, W., Liu, Y. Q., Shi, J., Starr, D., Tan, Q., Tao, Z. N., Zaitchik, B. F.,
629 Zavodsky, B., Zhang, S. Q., and Zupanski, M.: Integrated modeling of aerosol, cloud, precipitation and land processes at
630 satellite-resolved scales, Environ. Modell. Softw., 67, 149-159, 10.1016/j.envsoft.2015.01.007, 2015.
631 Petron, G., Granier, C., Khattatov, B., Lamarque, J. F., Yudin, V., Muller, J. F., and Gille, J.: Inverse modeling of carbon
632 monoxide surface emissions using Climate Monitoring and Diagnostics Laboratory network observations, J. Geophys.
633 Res.-Atmos., 107, 23, 10.1029/2001jd001305, 2002.
634 Petron, G., Granier, C., Khattatov, B., Yudin, V., Lamarque, J. F., Emmons, L., Gille, J., and Edwards, D. P.: Monthly CO
635 surface sources inventory based on the 2000-2001 MOPITT satellite data, Geophys. Res. Lett., 31, 5,
636 10.1029/2004gl020560, 2004.
637 Pielke, R. A., Cotton, W. R., Walko, R. L., Tremback, C. J., Lyons, W. A., Grasso, L. D., Nicholls, M. E., Moran, M. D.,
638 Wesley, D. A., Lee, T. J., and Copeland, J. H.: A COMPREHENSIVE METEOROLOGICAL MODELING SYSTEM -
639 RAMS, Meteorol. Atmos. Phys., 49, 69-91, 10.1007/bf01025401, 1992.
640 Pinder, R. W., Adams, P. J., Pandis, S. N., and Gilliland, A. B.: Temporally resolved ammonia emission inventories: Current
641 estimates, evaluation tools, and measurement needs, J. Geophys. Res.-Atmos., 111, 14, 10.1029/2005jd006603, 2006.
642 Randerson, J. T., Werf, G. R. v. d., Giglio, L., Collatz, G. J., and Kasibhatla, P. S.: Global Fire Emissions Database, Version
643 3 (GFEDv3.1). Data set. Available on-line [http://daac.ornl.gov/] from Oak Ridge National Laboratory Distributed Active
644 Archive Center, Oak Ridge, Tennessee, USA. doi:10.3334/ORNLDAAC/1191, 2013.
645 Rao, S. T., Galmarini, S., and Puckett, K.: Air Quality Model Evaluation International Initiative (AQMEII) Advancing the
646 State of the Science in Regional Photochemical Modeling and Its Applications, Bull. Amer. Meteorol. Soc., 92, 23-30,
647 10.1175/2010bams3069.1, 2011.
648 Saito, K., Fujita, T., Yamada, Y., Ishida, J. I., Kumagai, Y., Aranami, K., Ohmori, S., Nagasawa, R., Kumagai, S., Muroi, C.,
649 Kato, T., Eito, H., and Yamazaki, Y.: The operational JMA nonhydrostatic mesoscale model, Mon. Weather Rev., 134,
650 1266-1298, 10.1175/mwr3120.1, 2006.
651 Shao, M., Zhang, Y. H., Zeng, L. M., Tang, X. Y., Zhang, J., Zhong, L. J., and Wang, B. G.: Ground-level ozone in the Pearl
652 River Delta and the roles of VOC and NOx in its production, J. Environ. Manage., 90, 512-518,
653 10.1016/j.jenvman.2007.12.008, 2009.

Shen, J. L., Liu, X. J., Zhang, Y., Fangmeier, A., Goulding, K., and Zhang, F. S.: Atmospheric ammonia and particulate ammonium from agricultural sources in the North China Plain, Atmos. Environ., 45, 5033-5041, 10.1016/j.atmosenv.2011.02.031, 2011.

Sillman, S.: The relation between ozone, NOx and hydrocarbons in urban and polluted rural environments, Atmos. Environ., 33, 1821-1845, 10.1016/s1352-2310(98)00345-8, 1999.

Skamarock, W. C.: A description of the advanced research WRF version 3, Ncar Technical, 113, 7-25, 2008.

Stein, O., Schultz, M. G., Bouarar, I., Clark, H., Huijnen, V., Gaudel, A., George, M., and Clerbaux, C.: On the wintertime low bias of Northern Hemisphere carbon monoxide found in global model simulations, Atmos. Chem. Phys., 14, 9295-9316, 10.5194/acp-14-9295-2014, 2014.

Steinfeld, J. I.: Atmos. Chem. Phys.: From Air Pollution to Climate Change, Wiley, 1595-1595 pp., 1998.

Sun, W., Shao, M., Granier, C., Liu, Y., Ye, C. S., and Zheng, J. Y.: Long-Term Trends of Anthropogenic SO2, NOx, CO, and NMVOCs Emissions in China, Earth Future, 6, 1112-1133, 10.1029/2018ef000822, 2018.

Sun, Y. L., Wang, Z. F., Dong, H. B., Yang, T., Li, J., Pan, X. L., Chen, P., and Jayne, J. T.: Characterization of summer organic and inorganic aerosols in Beijing, China with an Aerosol Chemical Speciation Monitor, Atmos. Environ., 51, 250-259, 10.1016/j.atmosenv.2012.01.013, 2012.

Sun, Y. L., Wang, Z. F., Fu, P. Q., Yang, T., Jiang, Q., Dong, H. B., Li, J., and Jia, J. J.: Aerosol composition, sources and processes during wintertime in Beijing, China, Atmos. Chem. Phys., 13, 4577-4592, 10.5194/acp-13-4577-2013, 2013.

Tan, J., Fu, J. S., Carmichael, G. R., Itahashi, S., Tao, Z., Huang, K., Dong, X., Yamaji, K., Nagashima, T., Wang, X., Liu, Y., Lee, H. J., Lin, C. Y., Ge, B., Kajino, M., Zhu, J., Zhang, M., Hong, L., and Wang, Z.: Why models perform differently on particulate matter over East Asia? – A multi-model intercomparison study for MICS-Asia III, Atmos. Chem. Phys. Discuss., 2019, 1-36, 10.5194/acp-2019-392, 2019.

Tang, G., Wang, Y., Li, X., Ji, D., Hsu, S., and Gao, X.: Spatial-temporal variations in surface ozone in Northern China as observed during 2009-2010 and possible implications for future air quality control strategies, Atmos. Chem. Phys., 12, 2757-2776, 10.5194/acp-12-2757-2012, 2012.

Tang, X., Zhu, J., Wang, Z. F., and Gbaguidi, A.: Improvement of ozone forecast over Beijing based on ensemble Kalman filter with simultaneous adjustment of initial conditions and emissions, Atmos. Chem. Phys., 11, 12901-12916, 10.5194/acp-11-12901-2011, 2011.

Tang, X., Zhu, J., Wang, Z. F., Wang, M., Gbaguidi, A., Li, J., Shao, M., Tang, G. Q., and Ji, D. S.: Inversion of CO emissions over Beijing and its surrounding areas with ensemble Kalman filter, Atmos. Environ., 81, 676-686, 10.1016/j.atmosenv.2013.08.051, 2013.

Uno, I., He, Y., Ohara, T., Yamaji, K., Kurokawa, J. I., Katayama, M., Wang, Z., Noguchi, K., Hayashida, S., Richter, A., and Burrows, J. P.: Systematic analysis of interannual and seasonal variations of model-simulated tropospheric NO_2 in Asia and comparison with GOME-satellite data, Atmos. Chem. Phys., 7, 1671-1681, 10.5194/acp-7-1671-2007, 2007.

US EPA Office of Research and Development: CMAQv5.0, , doi:10.5281/zenodo.1079888, 2012.

688 Van Damme, M., Whitburn, S., Clarisse, L., Clerbaux, C., Hurtmans, D., and Coheur, P. F.: Version 2 of the IASI NH3 neural
689 network retrieval algorithm: near-real-time and reanalysed datasets, Atmos. Meas. Tech., 10, 4905-4914, 10.5194/amt-
690 10-4905-2017, 2017.
691 Van Damme, M., Clarisse, L., Whitburn, S., Hadji-Lazaro, J., Hurtmans, D., Clerbaux, C., and Coheur, P.-F.: Level 2 dataset
692 and Level 3 oversampled average map of the IASI/Metop-A ammonia (NH_3) morning column measurements (ANNI-
693 NH3-v2.1R-I) from 2008 to 2016. PANGAEA, 2018.
694 von Bobrutzki, K., Braban, C. F., Famulari, D., Jones, S. K., Blackall, T., Smith, T. E. L., Blom, M., Coe, H., Gallagher, M.,
695 Ghalaieny, M., McGillen, M. R., Percival, C. J., Whitehead, J. D., Ellis, R., Murphy, J., Mohacsi, A., Pogany, A.,
696 Junninen, H., Rantanen, S., Sutton, M. A., and Nemitz, E.: Field inter-comparison of eleven atmospheric ammonia
697 measurement techniques, Atmos. Meas. Tech., 3, 91-112, 10.5194/amt-3-91-2010, 2010.
698 Wang, G., Zhang, R., Gomez, M. E., Yang, L., Zamora, M. L., Hu, M., Lin, Y., Peng, J., Guo, S., and Meng, J.: Persistent
699 sulfate formation from London Fog to Chinese haze, Proc. Natl. Acad. Sci. U. S. A. of America, 113, 13630, 2016.
700 Wang, Z. F., Maeda, T., Hayashi, M., Hsiao, L. F., and Liu, K. Y.: A nested air quality prediction modeling system for urban
701 and regional scales: Application for high-ozone episode in Taiwan, Water Air Soil Pollut., 130, 391-396,
702 10.1023/a:1013833217916, 2001.
703 Warner, J. X., Wei, Z., Strow, L. L., Dickerson, R. R., and Nowak, J. B.: The global tropospheric ammonia distribution as seen
704 in the 13-year AIRS measurement record, Atmos. Chem. Phys., 16, 5467-5479, 10.5194/acp-16-5467-2016, 2016.
705 Warner, J. X., Dickerson, R. R., Wei, Z., Strow, L. L., Wang, Y., and Liang, Q.: Increased atmospheric ammonia over the
706 world's major agricultural areas detected from space, Geophys. Res. Lett., 44, 2875-2884, 10.1002/2016gl072305, 2017.
707 Xu, W., Wu, Q. H., Liu, X. J., Tang, A. H., Dore, A., and Heal, M.: Characteristics of ammonia, acid gases, and PM2.5 for
708 three typical land-use types in the North China Plain, Environ. Sci. Pollut. Res., 23, 1158-1172, 10.1007/s11356-015-
709 5648-3, 2016.
710 Xu, Z., Wang, T., Xue, L. K., Louie, P. K. K., Luk, C. W. Y., Gao, J., Wang, S. L., Chai, F. H., and Wang, W. X.: Evaluating
711 the uncertainties of thermal catalytic conversion in measuring atmospheric nitrogen dioxide at four differently polluted
712 sites in China, Atmos. Environ., 76, 221-226, 10.1016/j.atmosenv.2012.09.043, 2013.
713 Xu, Z., Liu, M., Zhang, M., Song, Y., Wang, S., Zhang, L., Xu, T., Wang, T., Yan, C., Zhou, T., Sun, Y., Pan, Y., Hu, M.,
714 Zheng, M., and Zhu, T.: High efficiency of livestock ammonia emission controls in alleviating particulate nitrate during
715 a severe winter haze episode in northern China, Atmos. Chem. Phys., 19, 5605-5613, 10.5194/acp-19-5605-2019, 2019.
716 Zhang, L., Wang, T., Zhang, Q., Zheng, J. Y., Xu, Z., and Lv, M. Y.: Potential sources of nitrous acid (HONO) and their
717 impacts on ozone: A WRF-Chem study in a polluted subtropical region, J. Geophys. Res.-Atmos., 121, 3645-3662,
718 10.1002/2015jd024468, 2016.
719 Zhang, L., Li, Q. Y., Wang, T., Ahmadov, R., Zhang, Q., Li, M., and Lv, M. Y.: Combined impacts of nitrous acid and nitryl
720 chloride on lower-tropospheric ozone: new module development in WRF-Chem and application to China, Atmos. Chem.
721 Phys., 17, 9733-9750, 10.5194/acp-17-9733-2017, 2017.

Zhang, L., Chen, Y. F., Zhao, Y. H., Henze, D. K., Zhu, L. Y., Song, Y., Paulot, F., Liu, X. J., Pan, Y. P., Lin, Y., and Huang, B. X.: Agricultural ammonia emissions in China: reconciling bottom-up and top-down estimates, Atmos. Chem. Phys., 18, 339-355, 10.5194/acp-18-339-2018, 2018.

Zhang, Q., Streets, D. G., Carmichael, G. R., He, K. B., Huo, H., Kannari, A., Klimont, Z., Park, I. S., Reddy, S., Fu, J. S., Chen, D., Duan, L., Lei, Y., Wang, L. T., and Yao, Z. L.: Asian emissions in 2006 for the NASA INTEX-B mission, Atmos. Chem. Phys., 9, 5131-5153, 10.5194/acp-9-5131-2009, 2009.

Zhang, Q., Pan, Y., He, Y., Zhao, Y., Zhu, L., Zhang, X., Xu, X., Ji, D., Gao, J., Tian, S., Gao, W., and Wang, Y.: Bias in ammonia emission inventory and implications on emission control of nitrogen oxides over North China Plain, Atmos. Environ., 214, 116869, https://doi.org/10.1016/j.atmosenv.2019.116869, 2019.

Zhao, Y., Zhou, Y. D., Qiu, L. P., and Zhang, J.: Quantifying the uncertainties of China's emission inventory for industrial sources: From national to provincial and city scales, Atmos. Environ., 165, 207-221, 10.1016/j.atmosenv.2017.06.045, 2017.

Zheng, B., Zhang, Q., Zhang, Y., He, K. B., Wang, K., Zheng, G. J., Duan, F. K., Ma, Y. L., and Kimoto, T.: Heterogeneous chemistry: a mechanism missing in current models to explain secondary inorganic aerosol formation during the January 2013 haze episode in North China, Atmos. Chem. Phys., 15, 2031-2049, 10.5194/acp-15-2031-2015, 2015.

Zheng, B., Chevallier, F., Ciais, P., Yin, Y., Deeter, M. N., Worden, H. M., Wang, Y. L., Zhang, Q., and He, K. B.: Rapid decline in carbon monoxide emissions and export from East Asia between years 2005 and 2016, Environ. Res. Lett., 13, 9, 10.1088/1748-9326/aab2b3, 2018.

Zheng, B., Chevallier, F., Yin, Y., Ciais, P., Fortems-Cheiney, A., Deeter, M. N., Parker, R. J., Wang, Y. L., Worden, H. M., and Zhao, Y. H.: Global atmospheric carbon monoxide budget 2000-2017 inferred from multi-species atmospheric inversions, Earth Syst. Sci. Data, 11, 1411-1436, 10.5194/essd-11-1411-2019, 2019.

Zhong, L. J., Louie, P. K. K., Zheng, J. Y., Wai, K. M., Ho, J. W. K., Yuan, Z. B., Lau, A. K. H., Yue, D. L., and Zhou, Y.: The Pearl River Delta Regional Air Quality Monitoring Network - Regional Collaborative Efforts on Joint Air Quality Management, Aerosol Air Qual. Res., 13, 1582-U1232, 10.4209/aaqr.2012.10.0276, 2013.

Zhong, Q. R., Huang, Y., Shen, H. Z., Chen, Y. L., Chen, H., Huang, T. B., Zeng, E. Y., and Tao, S.: Global estimates of carbon monoxide emissions from 1960 to 2013, Environ. Sci. Pollut. Res., 24, 864-873, 10.1007/s11356-016-7896-2, 2017.

Tables

Table 1: Basic configurations of participating models in MICS-Asia III

No	Horizontal resolution	Vertical resolution	First layer height	Horizontal advection	Vertical advection	Horizontal Diffusion	Vertical Diffusion	Gas phase chemistry	Aerosol processes	Dry depositiono f gases	Wet deposition of gases	Meteorology	Boundary condition	Online (Yes or No)
M1	45km	40σ_p level	57 m	Yamo (Yamartino, 1993)	ppm (Collella and Woodward, 1984)	multiscale	ACM2 (Pleim, 2007)	SAPRC99 (Carter, 2000)	Aero6 (Binkowski and Roselle, 2003)	Wesely (1989)	Henry's law	Standard[a]	GEOS-Chem (Martin et al., 2002)	No
M2	45km	40σ_p level	57 m	Yamo	ppm	multiscale	ACM2	SAPRC99	Aero6	Wesely (1989)	Henry's law	Standard[a]	Default	No
M3	45km	40σ_p level	57 m	Yamo	Yamo	multiscale	ACM2	CB05 (Yarwood et al., 2005)	Aero5	Wesely (1989)	Henry's law	Standard[a]	GEOS-Chem	No
M4	45km	40σ_p level	57 m	ppm	ppm	multiscale	ACM2_ inline	SAPRC99	Aero5	Wesely (1989)	Henry's law	Standard[a]	CHASER (Sudo et al., 2002a)	No
M5	45km	40σ_p level	57 m	ppm	ppm	multiscale	ACM2_ inline	SAPRC99	Aero5	M3DRY (Pleim et al., 2001)	Henry's law	Standard[a]	CHASER	No
M6	45km	40σ_p level	57 m	Yamo	Yamo	multiscale	ACM2_ inline	SAPRC99	Aero5	M3DRY	ACM	Standard[a]	CHASER	No
M7	45km	40σ_p level	29 m	Monotonic	Monotonic	no diffusion	no diffusion	RACM-ESRL with KPP (Goliff et al.,2013)	MADE (Ackerman n et al., 1998)	Wesely (1989)	Henry's law	WRF/NCEP[a]	Default	No
M8	45km	40σ_p level	57 m	5th order Monotonic	3th order Monotonic	MYJ	MYJ	RACM with KPP	MADE	Wesely (1989)	AQCHEM	WRF/NCEP[a]	CHASER	Yes
M9	45km	40σ_p level	16 m	5th order Monotonic	3th order Monotonic	Smagorinsk y first order closure	YSU (Hong et al., 2006)	RADM2 (Stockwell et al., 1990)	MADE	Wesely (1989)	Easter et al., (2004)	WRF/NCEP[a]	GEOS-Chem	Yes
M10	45km	60σ_p level	44 m	Monotonic	3th order Monotonic	2th order Monotonic	YSU	RADM2	GOCART	Wesely (1989)	Grell	WRF/ MERRA2[a]	MOZART + GOCART[b]	No
M11	45km	20σ_z level	50 m	Walcek and Aleksic (1998)	Walcek and Aleksic (1998)	multicale	K-theory	CBMZ (Zaveri et al.,1999)	ISORROPI A1.7 (Nenes et al.,1998)	Wesely (1989)	Henry's law	Standard[a]	CHASER	No

M12	45km	40 σ_p level	54 m	Walcek and Aleksic (1998)	Walcek and Aleksic (1998)	FTCS	FTCS	SAPRC99	Kajino et al. (2012)	Zhang et al. (2003)	Henry's law	Standard[a]	CHASER	No
M13	0.5°×0.667°	47σ_p level	60 m	ppm	ppm	Lin and McElroy, 2010	Lin and McElroy, 2010	NO_x-O_x-HC	ISORROPI A2.0 (Fountoukis and Nenes, 2007)	Wesely	Henry's law	GEOS-5[a]	Geos-Chem	No
M14	64km	15σ_z level	100 m	ppm	ppm	multiscale	ACM2	SAPRC99	ISORROPI A1.7	Wesely (1989)	Henry's law	RAMS/NCEP[a]	Geos-Chem	No

[a] Standard represents the reference meteorological field provided by MICS-Asia III project; WRF/NCEP and WRF/MERRA represents the meteorological field of the participating model itself, which was run by WRF driven by the NCEP and Modern Era Retrospective-analysis for Research and Applications (MERRA) reanalysis dataset. RAMS/NCEP is the meteorology field run by RAMS driven by the NCEP reanalysis dataset.

[b] Boundary conditions of M10 are from MOZART and GOCART (Chin et al., 2002; Horowitz et al.,2003), which provided results for gaseous pollutants and aerosols, respectively.

767 **Table 2: Statistics of simulated annual mean concentrations over the NCP and PRD regions.**

Species	Regions	Statistics	Model													
			M1	M2	M4	M5	M6	M7	M8	M9	M10	M11	M12	M13	M14	Ense
NO_2	NCP	R(spatial)[a]	0.63	0.67	0.67	0.67	0.67	0.70	0.70	0.59	0.57	0.66	0.69	-	0.70	0.67
		R(temporal)[b]	0.82	0.92	0.93	0.86	0.92	0.81	0.28	0.85	0.95	0.75	0.90	-	0.96	0.91
		MBE	-4.11	-5.66	-6.54	1.86	-5.12	-5.04	3.30	8.28	-2.45	0.00	-3.81	-	-2.99	-1.86
		NMB(%)	-17.8	-24.5	-28.4	8.0	-22.2	-21.9	14.2	35.9	-10.6	0.02	-16.5	-	-13.0	-8.0
		RMSE	7.40	8.25	8.79	6.75	8.01	7.55	6.54	12.74	7.72	6.37	7.38	-	6.68	6.36
	PRD	R(spatial) [a]	0.12	0.06	0.07	0.07	0.06	0.12	0.20	0.38	0.00	0.08	0.12	-	0.02	0.10
		R(temporal)[b]	0.93	0.80	0.86	0.88	0.79	0.68	0.83	0.95	0.74	0.74	0.75	-	0.52	0.86
		MBE	-6.73	-9.84	-7.21	1.96	-6.66	-3.99	3.24	-7.61	-1.84	3.02	-5.49	-	-5.03	-3.85
		NMB(%)	-30.1	-44.0	-32.3	8.8	-29.8	-17.9	14.5	-34.0	-8.2	13.5	-24.6	-	-22.5	-17.2
		RMSE	11.31	13.14	12.00	10.80	11.84	10.60	8.73	10.69	10.72	10.51	11.68	-	12.00	10.15
CO	NCP	R(spatial) [a]	0.35	0.48	0.27	0.34	0.36	0.22	0.19	0.48	0.49	0.33	0.35	-0.13	0.29	0.37
		R(temporal)[b]	0.94	0.96	0.92	0.22	0.90	0.77	0.94	0.92	0.82	0.85	0.94	0.85	0.88	0.92
		MBE	-1.53	-1.35	-1.59	-1.69	-1.52	-1.64	-1.29	-1.16	-1.55	-1.37	-1.38	-1.53	-1.51	-1.47
		NMB(%)	-68.9	-60.9	-71.4	-76.2	-68.2	-73.7	-58.2	-52.0	-70.0	-61.6	-62.3	-68.9	-68.0	-66.2
		RMSE	1.71	1.54	1.77	1.86	1.70	1.82	1.51	1.36	1.74	1.57	1.58	1.74	1.70	1.66
	PRD	R(spatial) [a]	0.04	-0.24	-0.25	-0.23	-0.22	-0.05	0.08	0.55	-0.02	-0.01	-0.22	0.09	-0.21	-0.06
		R(temporal)[b]	0.96	0.91	0.93	0.84	0.95	0.90	0.90	0.96	0.83	0.87	0.93	0.76	0.82	0.94
		MBE	-0.66	-0.64	-0.65	-0.64	-0.62	-0.64	-0.51	-0.57	-0.50	-0.51	-0.58	-0.52	-0.67	-0.59
		NMB(%)	-68.4	-67.0	-67.0	-66.7	-64.7	-66.5	-53.3	-59.7	-52.3	-52.7	-60.7	-54.1	-69.6	-61.7
		RMSE	0.70	0.70	0.70	0.69	0.67	0.69	0.57	0.62	0.56	0.57	0.64	0.58	0.72	0.65
NH_3	NCP	R(spatial)[a]	0.72	0.70	0.69	0.70	0.71	0.65	-	0.70	0.57	0.62	0.67	0.61	0.58	0.69
		R(temporal)[b]	-0.48	-0.22	-0.45	-0.55	-0.41	0.04	-	-0.19	0.64	0.08	-0.37	0.65	-0.04	-0.17
		MBE	-0.69	2.95	-6.14	-6.61	-3.89	4.94	-	21.8	10.5	-0.07	0.31	-5.19	-12.2	0.47
		NMB(%)	-3.8	16.1	-33.5	-36.0	-21.2	26.9	-	118.7	57.1	-0.4	1.69	-28.3	-66.3	2.59
		RMSE	7.20	10.04	8.95	9.24	7.48	8.78	-	29.24	13.48	8.30	7.33	8.82	14.48	7.20

768 [a] R(spatial) represents the spatial correlation coefficients between simulated and observed concentrations sampled from different stations in NCP or PRD;

769 [b] R(temporal) represents the temporal correlation coefficients between simulated and observed monthly mean concentrations from January to December in 2010;

770

Figures

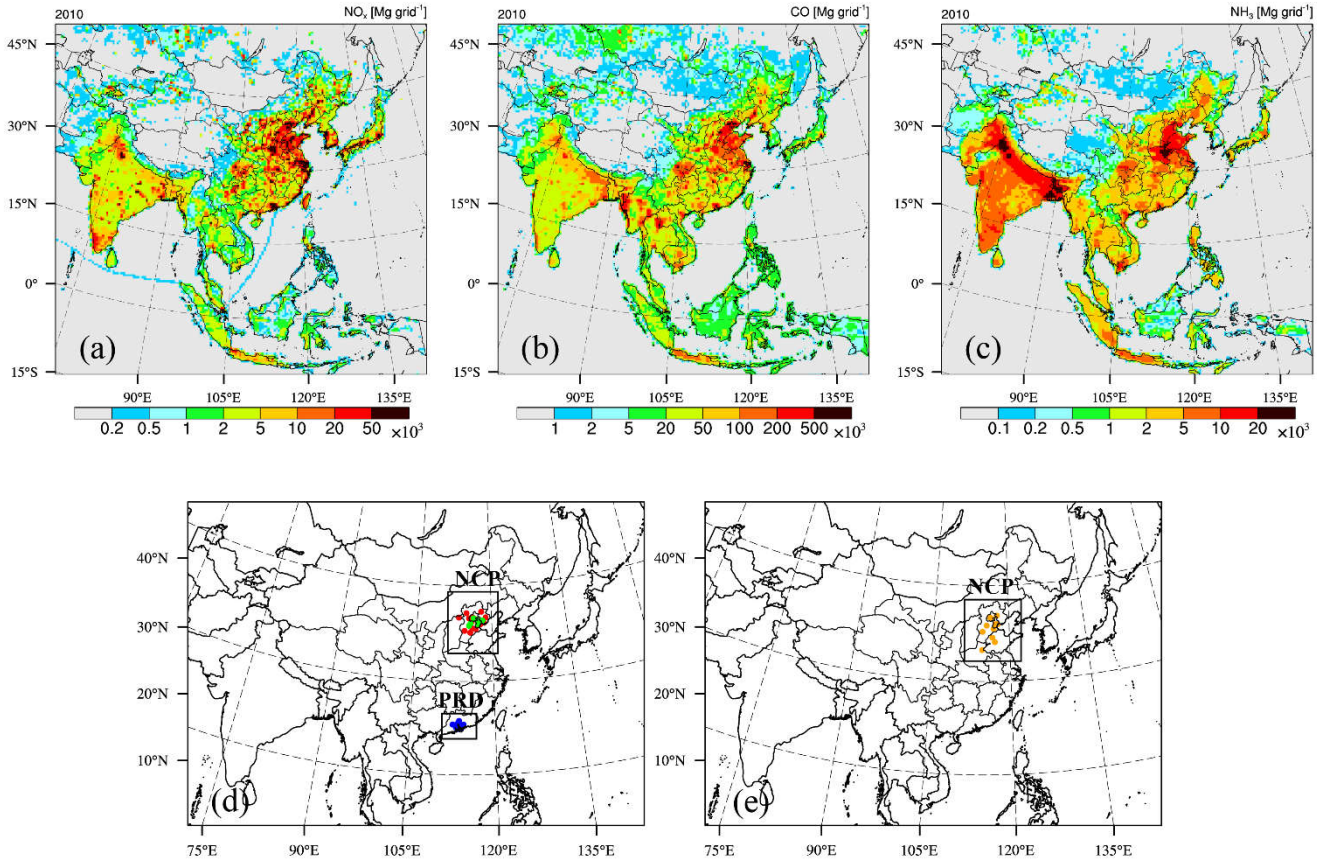

Figure 1: Modeling domains of the participated models except M13 and M14 along with spatial distributions of the total emissions of (a) NO_x, (b) CO and (c) NH_3 in 2010 provided by MICS-Asia III (upper panel), and the distributions of observation stations of (d) NO_2 and CO over the NCP and PRD regions, as well as (e) NH_3 over the NCP region (lower panel). The horizontal resolution is 45km×45km. Note that domains of M13 and M14 are shown in fig. 7 and only six of nineteen observational sites (green) over the NCP region have CO measurements.

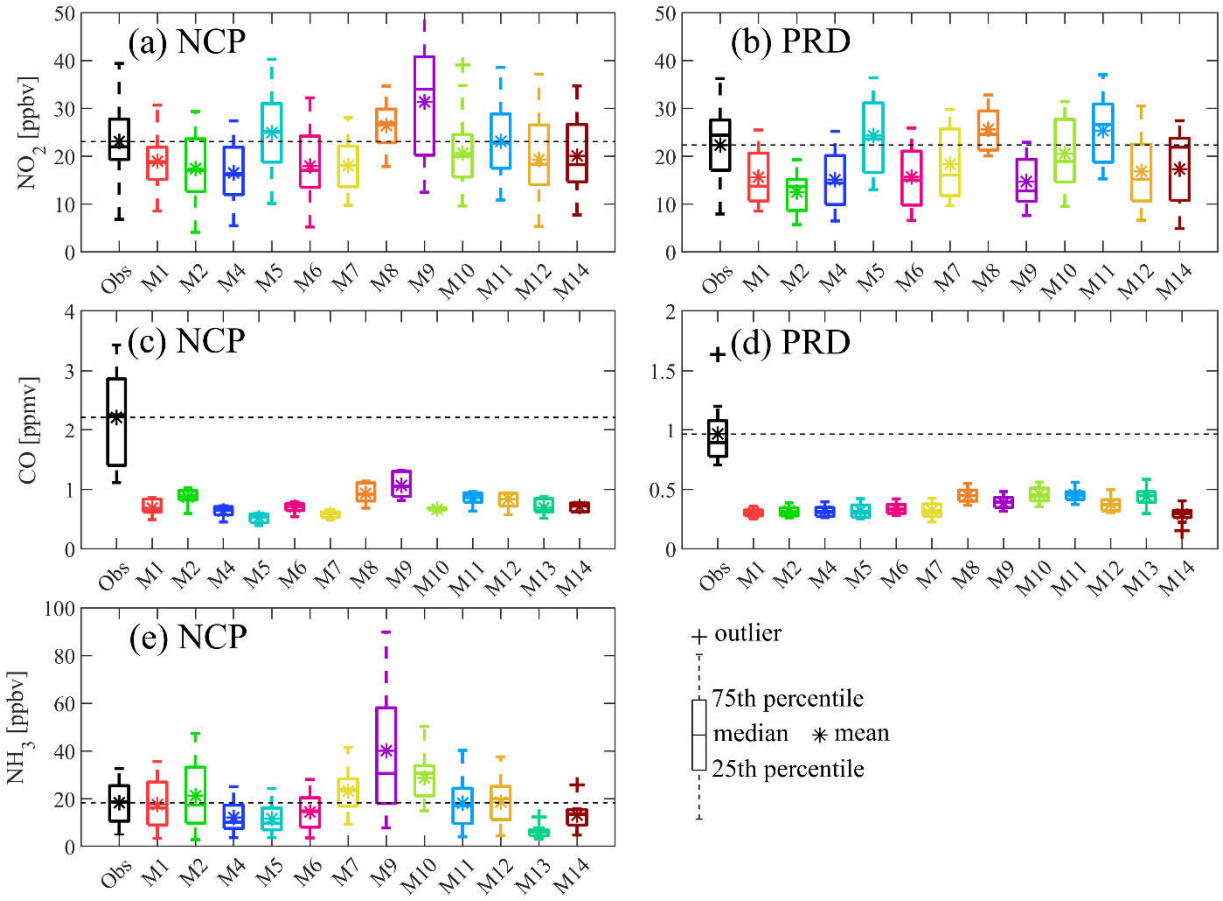

778

779 **Figure 2: Boxplot of simulated and observed annual mean NO_2, CO and NH_3 concentrations sampled from different stations over**
780 **the NCP (a, c, e) and PRD (b, d) regions. The outlier was defined as values larger than $q_3 + 1.5 \times (q_3 - q_1)$ or less than $q_1 -$**
781 **$1.5 \times (q_3 - q_1)$, where q_3 denotes the 75th percentile, and q_1 the 25th percentile. This approximately corresponds to 99.3 percent**
782 **coverage if the data are normally distributed.**

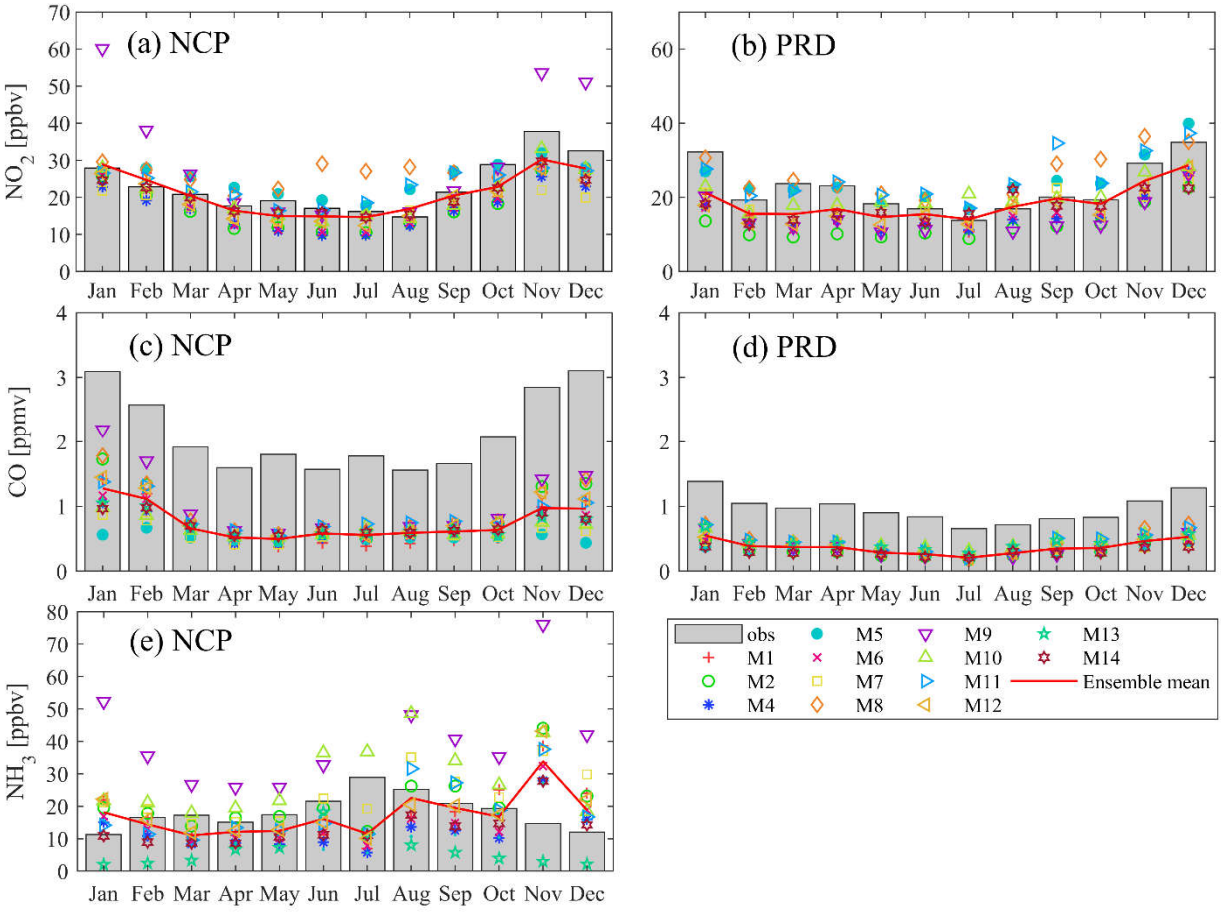

783

784 **Figure 3: Timeseries of regional mean NO_2, CO concentrations over the NCP (a, c) and PRD (b, d) regions as well as NH_3**
785 **concentrations over the NCP (e) region from January to December in year 2010.**

786

787

788

789

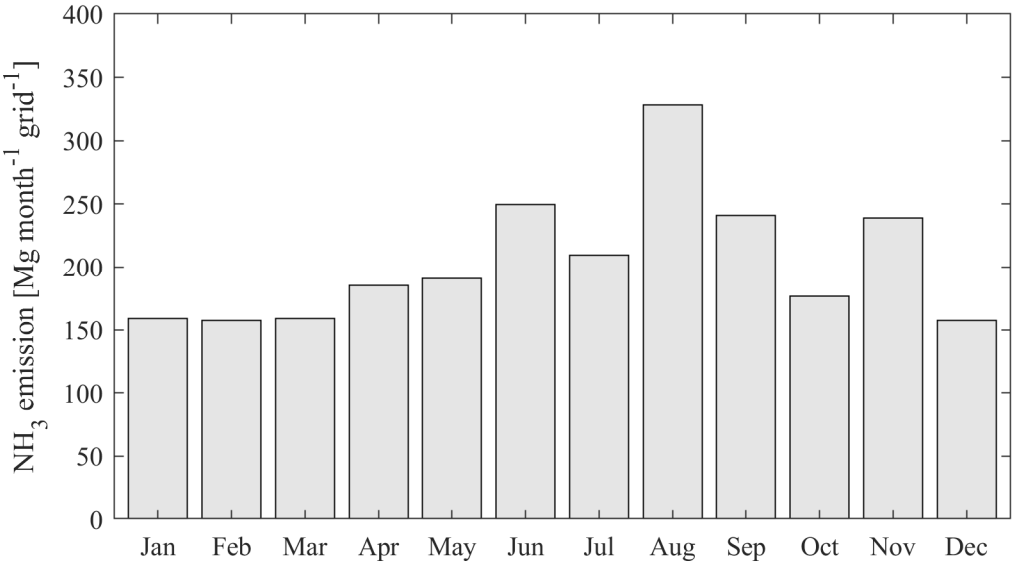

790

791 **Figure 4: Timeseries of NH_3 emissions over the NCP region provided by MICS-Asia III on a horizontal resolution of 45km×45km**
792 **from January to December in year 2010.**

793

794

795

796

797

798

799

800

801

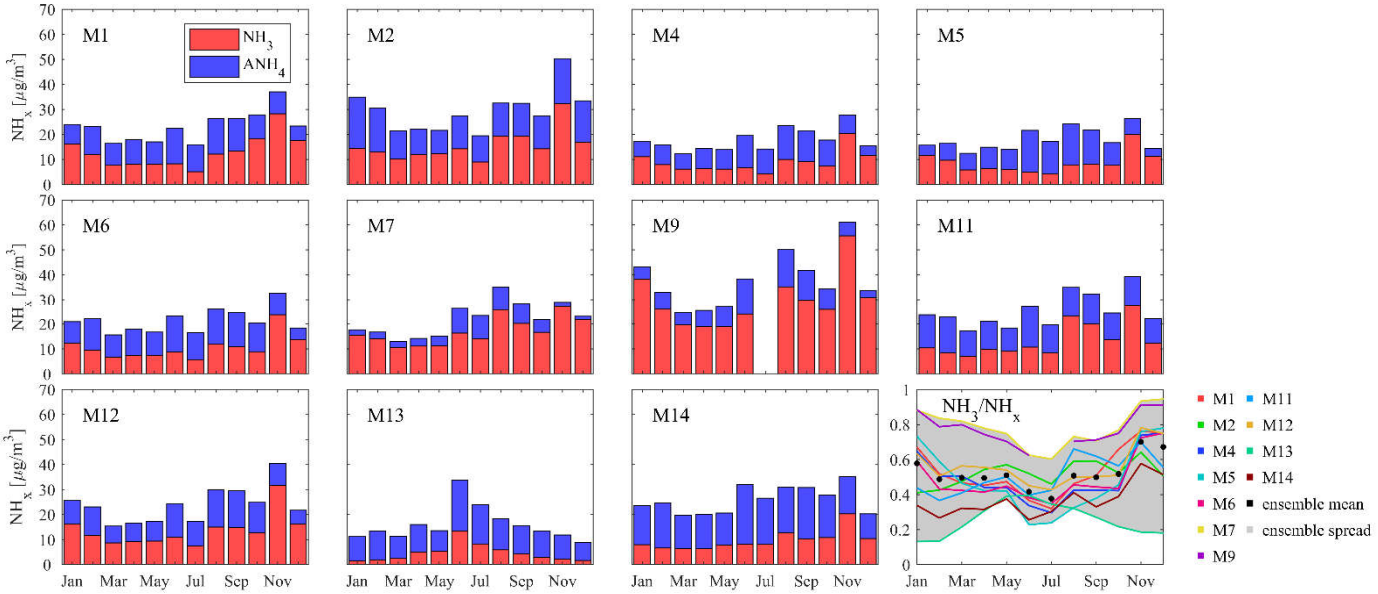

Figure 5: Timeseries of the multi-model simulated total ammonium (NH_x = NH_3 + NH_4^+) in atmosphere along with the ratio of gaseous NH_3 to the total ammonium over NCP from January to December in year 2010.

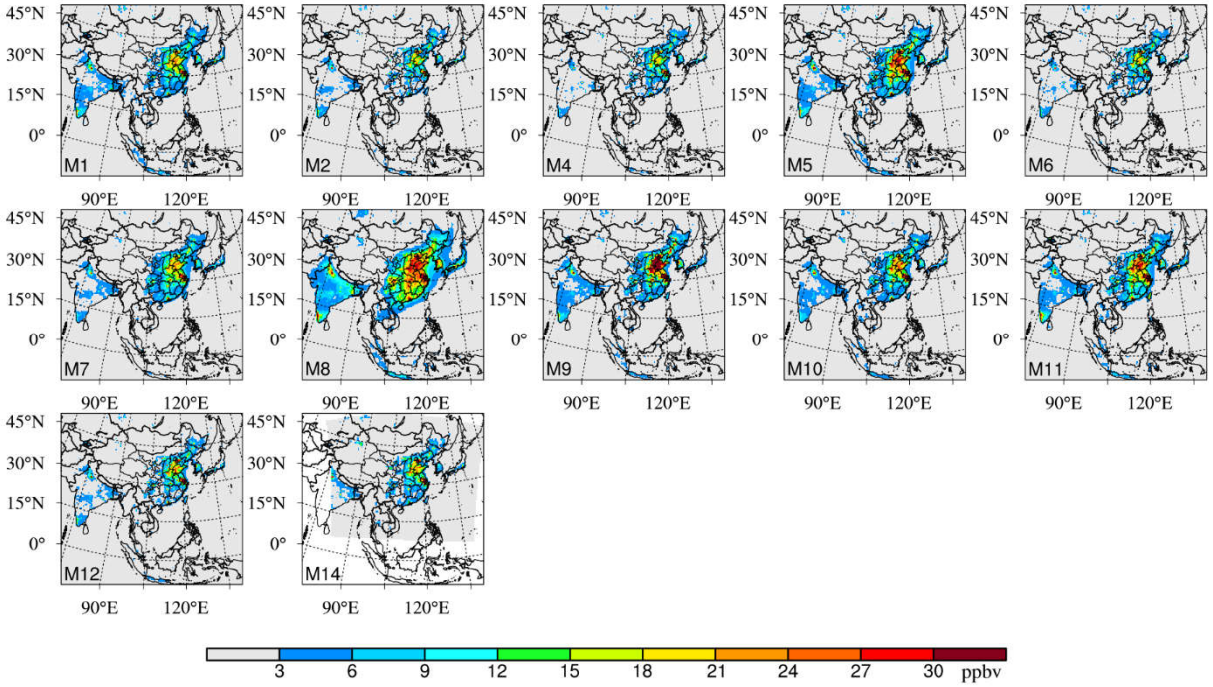

814

815 **Figure 6: Spatial distribution of the annual mean NO_2 concentrations from each modeling results of MICS-Asia III. Note that M13**
816 **are not included in this figure.**

817

818

819

820

821

822

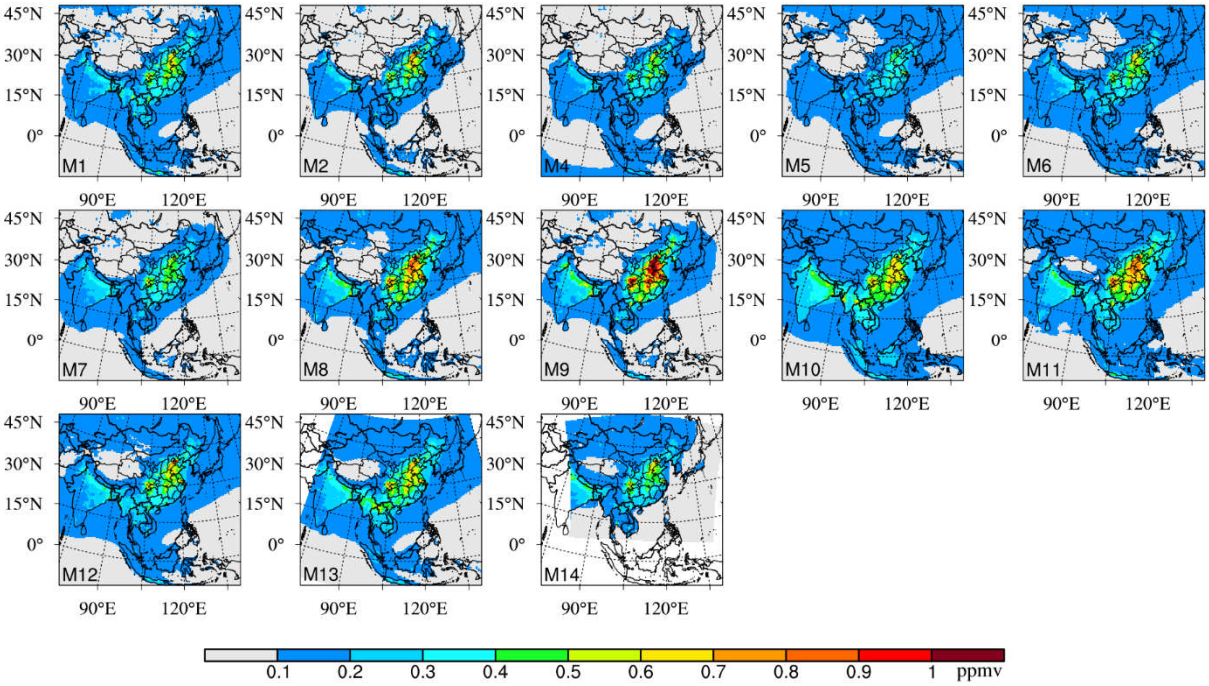

Figure 7: Spatial distribution of the annual mean CO concentrations from each modeling results of MICS-Asia III.

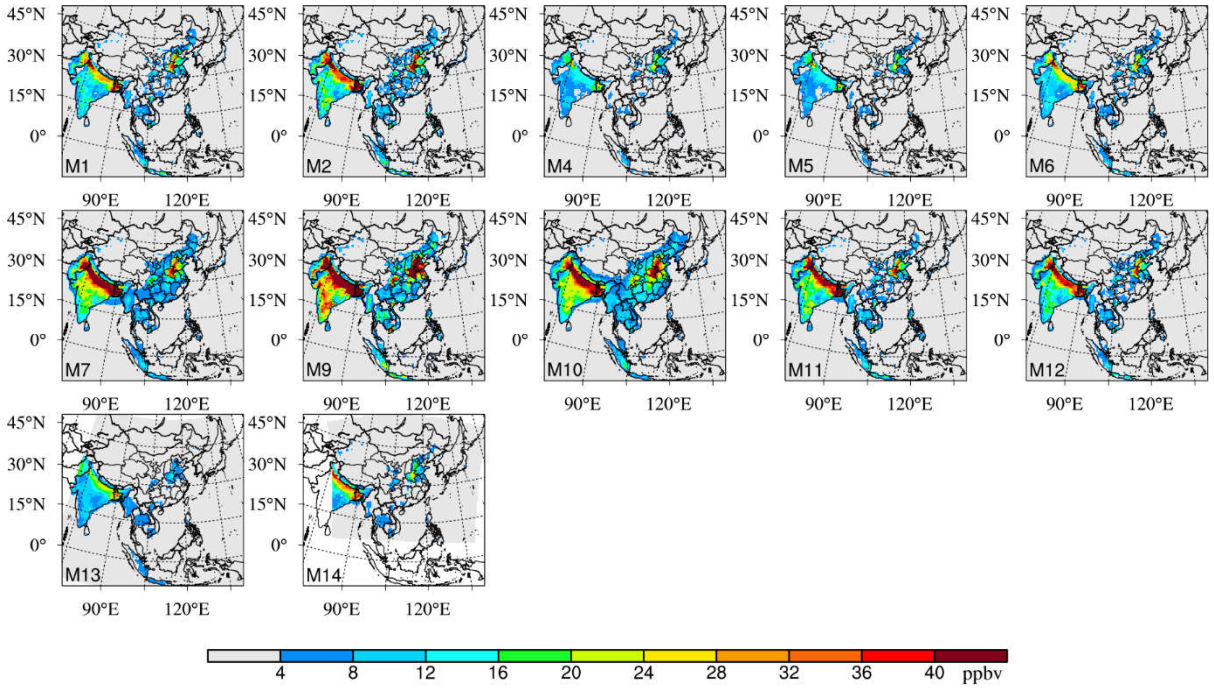

832

833 **Figure 8: Spatial distribution of the annual mean NH_3 concentrations from each modeling results of MICS-Asia III.**

834

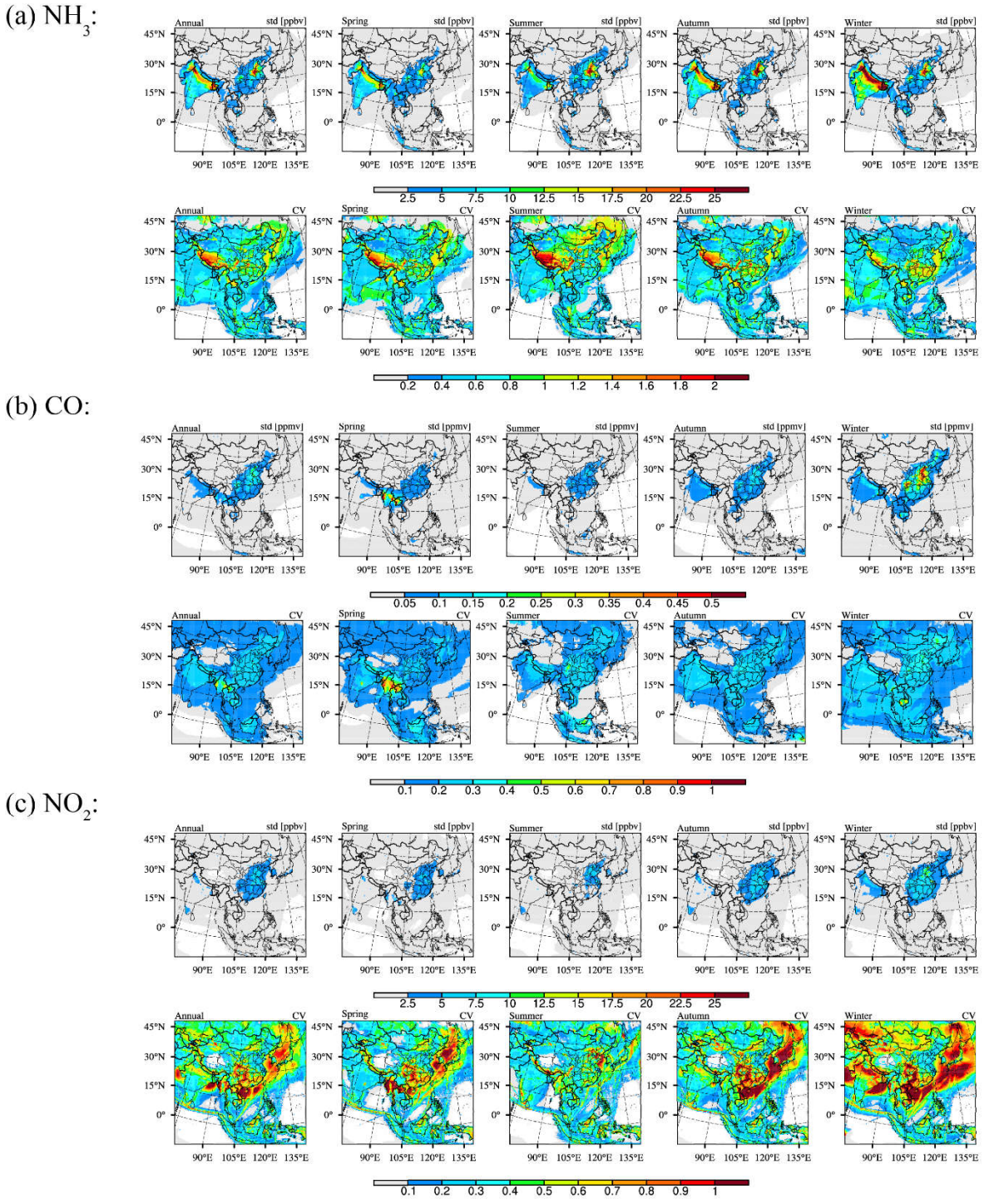

Figure 9: Spatial distribution of the standard deviation of (a) NH_3, (b) CO and (c) NO_2 multi-model predictions in MICS-Asia III, as well as the corresponding distribution of CV on the annual and seasonal basis.